UNIVERSITY OF TWENTE.

Faculty of Engineering Technology -
Biomechanical Engineering

Soft Robotics Joystick using 3-D Printed Piezoresistive Sensors with Digital Avatar Interface.

Matthijs A. Aldenkamp

Bachelor Assignment
February 2024

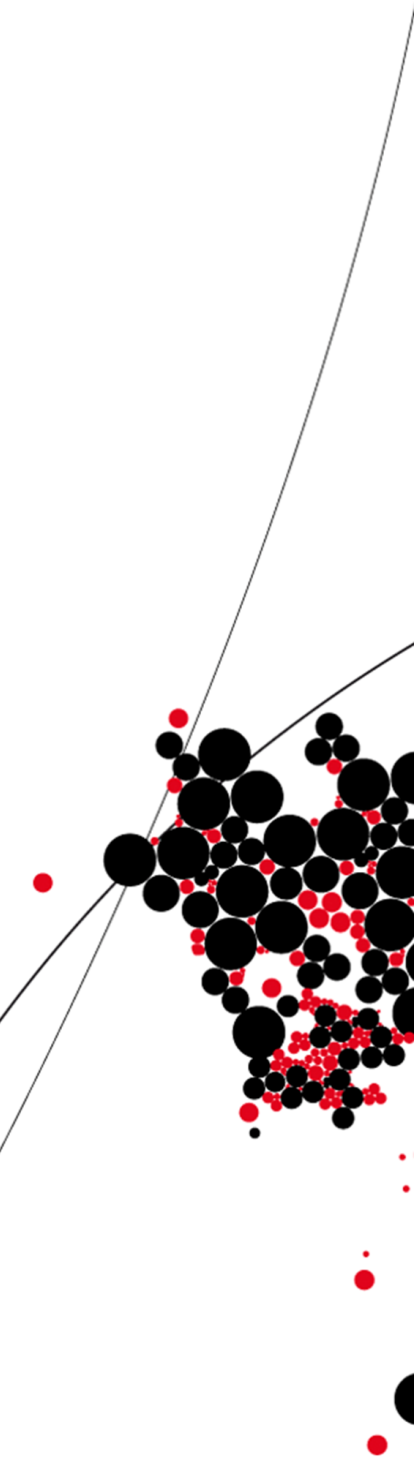

Supervisors:
Dr. A. Sadeghi
Ir. N. Willemstein
External Committee Member
Dr. I. Tamadon

Soft Robotics Lab
Dept. of Biomechanical Engineering
Faculty of Engineering Technology
University of Twente
P.O. Box 217
7500 AE Enschede
The Netherlands

Contents

Abstract ii

Acronyms iii

1 Introduction 1

2 Materials and Methods 3
- 2.1 General Setup . . . 3
- 2.2 Body of the Joystick . . . 3
- 2.3 Joystick Fabrication . . . 5
- 2.4 Conductive Thermoplastic sensor application . . . 6
- 2.5 Digital Avatar . . . 8
- 2.6 Data Acquisition and Processing . . . 10

3 Results and Discussion 13
- 3.1 Physical Joystick . . . 13
- 3.2 Sensor Resistance Data . . . 14
- 3.3 Avatar Interface . . . 19
- 3.4 Validation . . . 22

4 Conclusions 23
- 4.1 Joystick . . . 23
- 4.2 Sensor Data and Avatar Interface . . . 23
- 4.3 Recommendations . . . 23

References 24

Appendices

A Printing issues 26

B Extra Result Graphs 29

C Used software 38

Abstract

Soft robotics are a field of robotics that, due to the flexibility, compliance, and adaptability of soft robots to changing environments, has significant advantages over rigid robotics. One important aspect of this is the possibility to use soft robotics where interaction with humans or delicate objects is required, including use in minimally invasive surgery. An important existing technology for this purpose is flexible endoscopes. These use a controller to bend and manipulate the device and while effective, it cannot take advantage of another important property of soft robots: their infinite degrees of freedom.

This thesis investigates the use of the piezoresistive qualities of conductive thermoplastic polyurethane composite materials to detect the change of geometry of a bellow, and to derive the angles to reconstruct the joystick in a digital avatar. To do this, a joystick is 3-D printed out of non-conductive thermoplastic polyurethane, upon which the piezoresistive sensors are printed directly. To print these sensors, Matlab is used to write the g-code needed to follow the geometry of the bellows of the joystick. The avatar is constructed using a partial torus for each bellow, and a combination of an Arduino, an analog to digital converter, and a multiplexer are used to read the sensor data. Simple calculations are then used to derive the angles used to interface with the avatar.

The sensor data acquired from the experiments that were conducted were inconsistent, but clearly showed recognisable resistance profiles which could be used reconstruct the joystick in the avatar, both the halves of the joystick separately and both halves combined. Most of the unwanted signal behaviour could be attributed to previously studied phenomena, such as the piezoresistivity and the viscoelastic properties of the materials. The joystick constructed in this thesis is a successful proof of concept for the use of geometry specific specific piezoresistive sensor and demonstrates the potential for infinite degree of freedom teleoperation of soft robotics devices.

List of acronyms

DOF Degrees of Freedom

MIS Minimally Invasive Surgery

TPU Thermoplastic Polyurethane

PLA Polylactic Acid

FMD Fused Deposition Modeling

CB Carbon Black

CTPUC Conductive Thermoplastic Polyurethane Composite

ADC Analog to Digital Converter

I^2C Inter-Integrated Circuit

1 Introduction

Soft Robotics is a field of robotics that deals with the use of soft materials as opposed to rigid materials in robotics. Due to the mechanical flexibility and compliance of soft robots, they have the potential to outperform rigid robots in applications with varying environments and conditions [1]. These qualities also make it possible to use Soft Robotics in applications where interaction with humans or delicate objects is required, as they present fewer risks of harm than using rigid robots. Examples of possible functions are locomotion [2], manipulation [3] and application in healthcare [4] [5].

Soft Robotics already has use cases in healthcare [1], one of which is using endoscopes in Minimally Invasive Surgery (MIS) [6]. Endoscopes (see figure 1) are essentially flexible tubes [4] with a camera that is used to look inside the human body during surgery. They use a handheld controller operated by a surgeon, which is used to manipulate the shape of the device during endoscopies and MISs. This allows for greater freedom of movement than rigid alternatives, allowing surgeons to reach some internal structures without making any incisions [5].

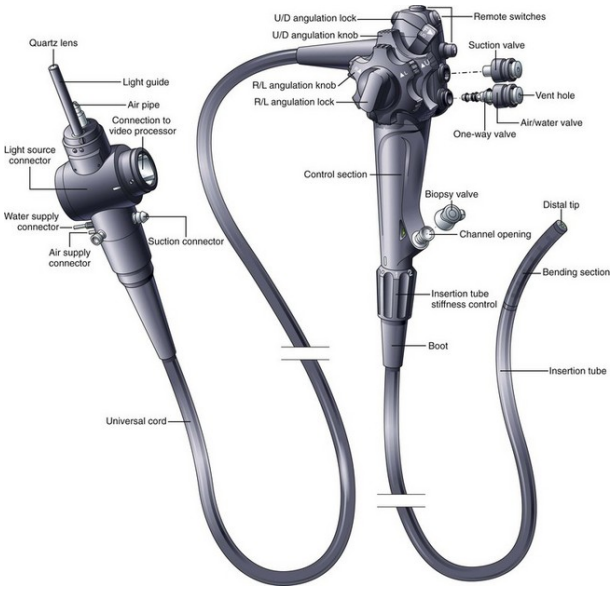

Figure 1 The standard layout of a flexible endoscope [7]

While using the currently standard controller for operation of rigid and limited flexibility endoscopes works, as is made evident by their widespread use, it does not fully take advantage of another core feature of soft robotics: infinite Degrees of Freedom (DOF). Soft robots are continuously manipulable over their structure, which gives them infinite DOF. The limited number of possible inputs makes it impossible to take full advantage of a soft robot's DOF in manual control. Instead, a controller used for soft robotics must be as continuously manipulable as the robot itself..

Using the full capabilities of infinite DOF in robots gives the operator far greater freedom in the operation of the robot, allowing them access to harder to reach places and to manipulate objects [1] where it would otherwise have been impossible. To this end, controllers must be created which can take advantage of these qualities of Soft Robotics. Steps have already

been made towards sensing the manipulation of soft structures using its own geometry [8] and teleoperation using a soft joystick [9]. However, there is currently no controller that can sense both its own geometry and use this to operate a soft robot, which is what is aimed to achieve in this thesis.

Producing such a joystick presents several challenges. These include the production of the joystick itself, attaching a method of sensing the manipulation of the joystick, and providing a way to visualise the sensor output by means of a digital avatar.

This thesis proposes solutions for all these challenges. Firstly, the joystick that is produced for this paper is entirely 3-D printable. This makes it easy to (re)produce, and a cost effective device that can be made with a very small number of tools.

Secondly, the sensors of the device are 3-D printed directly onto the body of the joystick, requiring no further tools than the printer the rest of the joystick was made with. The sensor material is piezoresistive, which will allow the resistance of these sensors to change as the joystick is manipulated, making it possible to derive its bending profile.

Thirdly, a digital avatar was constructed which allows for the visualisation of the data. This makes it possible to intuitively validate the sensor's outputs. With all these elements combined, this thesis proposes a proof of concept for the use of geometry specific soft joystick towards fully continuous soft robotics teleoperation.

2 Materials and Methods

2.1 General Setup

The joystick and avatar need to be integrated before being usable as an instrument for MIS. An example of this can be seen in figure 2. This integration requires several components, each of which will be essential for the next step in the sequence. The main structure of the flexible, haptic joystick must be designed and produced, as well as any connecting pieces. Sensors must be attached to the joystick to be able to make it produce an output. The sensor output data must read and processed. Finally, to show that the data is actually related to the joystick's bending by the user, an avatar must be made to visualise the translation of actual bending to digital, usable output. Finally, to demonstrate that it is possible to use the sensor data to derive the configuration of the joystick, an avatar must be made to visualise the translation of physical bending to digital bending.

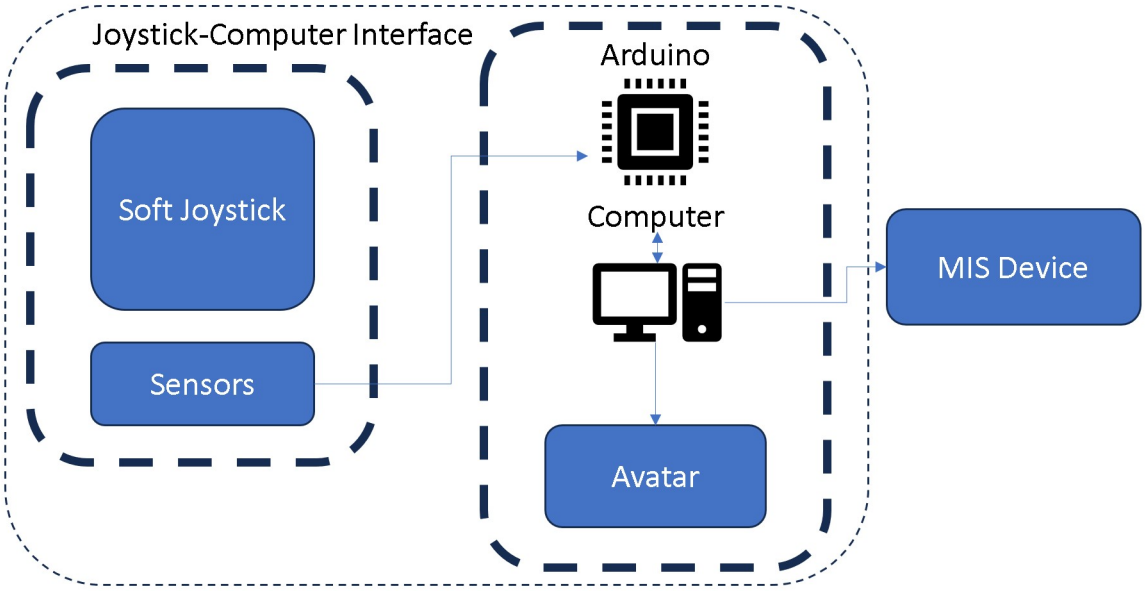

Figure 2 The setup for the soft joystick-computer interface.

2.2 Body of the Joystick

To ensure the setup can take user and be operated by a user, a flexible joystick was realised, which will also become the foundation for the sensors to be placed upon. The joystick consists of two bellows connected by smaller, rigid connection pieces. The joystick is mounted to a surface using mounting pieces similar to the connectors.

The main criteria for the bellows were that they could be bent to an angle of approximately 90°, and that it was 3D-printable. The bending angle was achieved by use of bellows. This allows for for the joystick's structure to buckle selectively, which is used for the controlled bending of the device. This buckling along with the shape and material contact of the corrugations of the bellows are also used in the sensor principle as explained in section 2.6. The dimensions were chosen empirically, and can be seen in figure 3a. A corrugation angle of 70° was found to work

appropriately both for the selective buckling and making it 3-D printable. Furthermore, the ends of the bellows were designed to be octagonal. This shape provided an simple, symmetrical foundation for easy application of the sensor material while providing ample anchorage against twisting of the joystick within the connectors. The ends of the top bellow are nearly identical, with the exception of the removal of the circular groove. A simplified view of these ends can be seen in figure 3b.

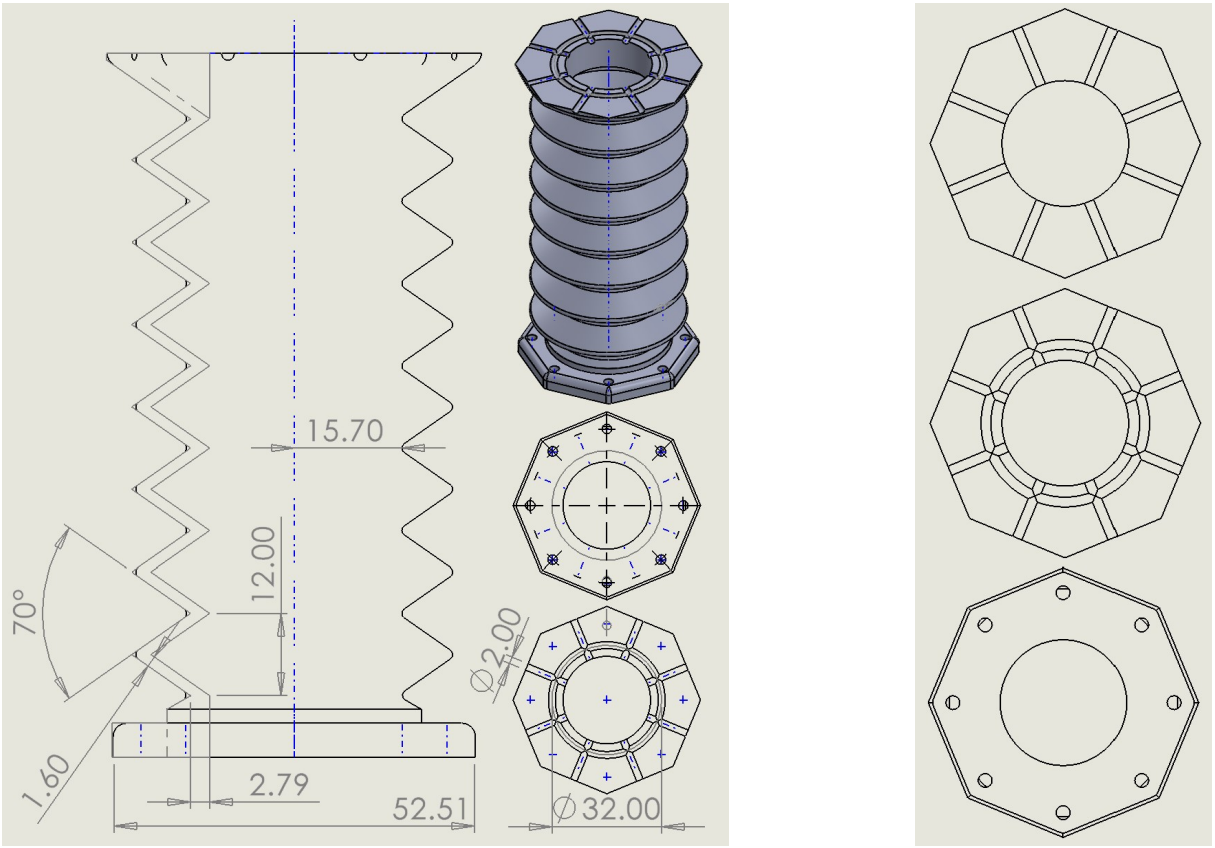

(a) **(b)**

Figure 3: (a): SolidWorks drawings and designs for the bottom bellows. All dimensions are given in mm with the exception of the corrugation angle. (b): A simplified view of the bellow ends, in order of placement. The middle bellow end is identical in the top of the first bellow and the bottom of the second bellow.

The connection pieces for the joystick included mounting pieces, connectors, and an end cap (see figure 4). The mounting pieces were used to attach the bottom bellow to the base. The connectors were used to connect the two bellows in the middle. The end piece was a simple cap which, combined with connectors, provided a terminal at the end for attachments. This end cap also partially prevented the electronics at the end of the Joystick from making contact with the skin of the operator, which could cause noise in the signal of the sensor.

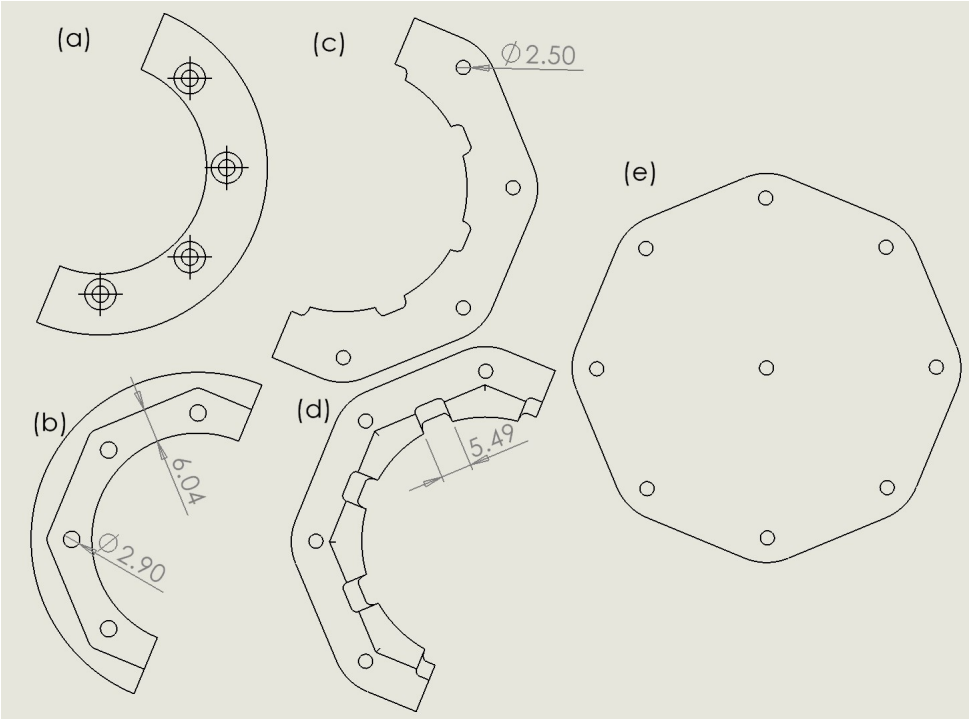

Figure 4: The connection pieces, with all dimensions in mm. (a),(b): The top and bottom view of the mounting pieces respectively. (c),(d): The top and bottom view of the connectors respectively. (d): a bottom view of the end cap.

2.3 Joystick Fabrication

The bellows are designed using SolidWorks 2022 (Dassault Systèmes, France) and printed using Fused Deposition Modeling (FMD) 3D printing on the Ender 5 (Creality, China) platform using NinjaFlex (NinjaTek, USA) [10] Thermoplastic Polyurethane (TPU) filament, 0.8mm printing nozzle and a printing temperature of 230°C.

Working with TPU as a printing material for a thin, tall structure (see figure 3a) presents issues during the print. The greatest of these is the amount of wobble of the printed material as subsequent layers are printed, and this issue increases as the structure becomes taller. To mitigate this, supports were printed from Polylactic Acid (PLA) (see figure 5) to place around the bellow during the print. These supports were made as a shell of the bellow to provide maximum support in all directions and to make them usable secondarily as holding blocks for the bellows during the application of the conductive polymer.

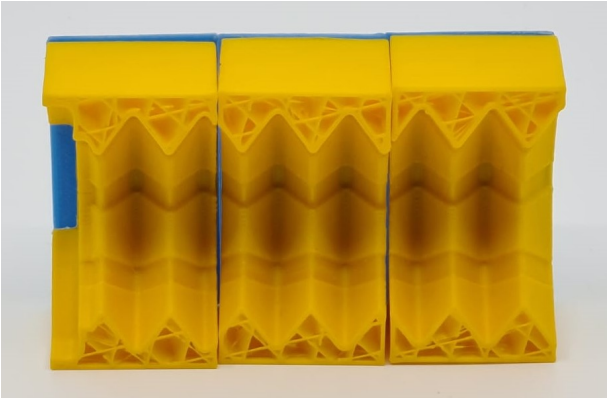

Figure 5 The empty supports for the bellows, as viewed from the top.

2.4 Conductive Thermoplastic sensor application

With the main body of the joystick, a method of measuring its orientation is required to allow the joystick to interface with the digital avatar. For this reason, four strips of equidistant Conductive Thermoplastic Polyurethane Composite (CTPUC) were added to the outer walls of the bellows. The chosen thermoplastic was NinjaTek's Eel [11]. This material contains Carbon Black (CB) which makes it conductive. Its piezoresistive characteristics lead to changes in resistance as the material is stretched and compressed. When the bellow is compressed, the CTPUC is likewise compressed. Furthermore, when the corrugations of the bellow are collapsed, the CTPUC on its walls make contact (see figure 6), reducing the distance the current has to travel through the resistive material.

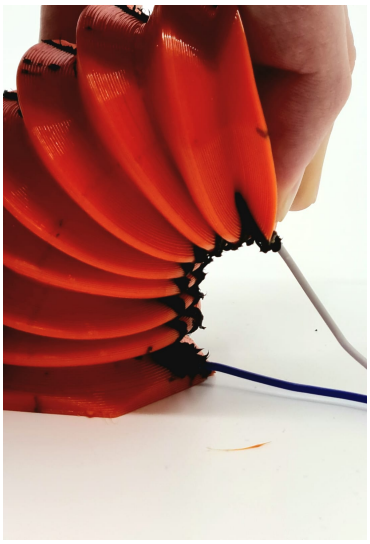

Figure 6 A prototype bellow as it is bent. The black material on the bellows is the CTPUC.

In order to re-use the supports used in section 2.2 as holding mounts to keep the bellow steady as the CTPUC is printed, grooves were added to these supports which give space for the CTPUC (see figure 5). These supports and a visualisation of their function can be seen in figure 7. Grooves were added in the connection pieces as well to give room for the sensor material.

Figure 7

Figure 8 The bottom bellow in the PLA supports, viewed from the top of the bellow.

To apply the CTPUC to the printed bellows, G-code was written to follow the path of the bellow's corrugations. The parameters of this path were determined empirically. These adjustments were facilitated by making videos of the printer's path without extruding filament, until a suitable path was produced. Because rapid iteration was desirable, the G-code was written iteratively using MATLAB (MathWorks, USA). The path the printer took was the same on each corrugation, moving from right to left from the camera's point of view (see figure 9a), and was as follows:

1. Move to the middle of the corrugation.
2. Move down into the dip of the corrugation.
3. Print up slope to the right.
4. "Cut off" the filament by moving diagonally past the corrugation top, then move up,then left to return.
5. Move to the middle of the corrugation.
6. Move down into the dip of the corrugation.
7. Print up the slope to the left.
8. "Cut off" the filament by moving diagonally past the corrugation top, then move up,then right to return..
9. Repeat step 1-8 on subsequent corrugations.

Rather than printing one continuous path along the bellows, this path was chosen as the printing nozzle would drag through the filament as it was printing, producing inconsistent results as well as stringing of the CTPUC.

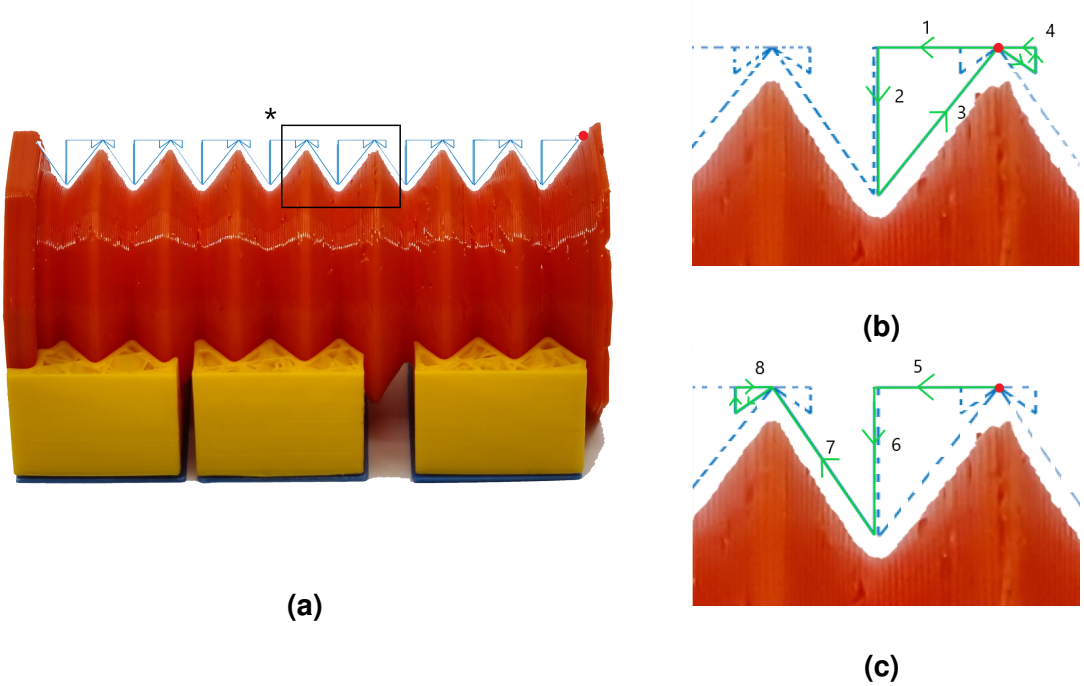

Figure 9: a: The print path over the bellow, moving from right to left. b: Step 1-4. c: step 5-8 in the same corrugation.

A graphical representation of the programmed path can be seen in figure 9, where step 1-4 can be seen in figure 9b, and step 5-8 can be seen in figure 9c. There is a slight difference in the paths down into the dip of the corrugation, which was done to prevent the nozzle pressing down into the previously printed filament, which would also cause stringing.

2.5 Digital Avatar

In order to provide an intuitive graphical representation of the joystick, a digital avatar was created in MATLAB [12]. By plotting a section of a torus, the visualisation of a bent rod can be produced. Rotation matrices can later be utilised to make the avatar assume any possible orientation and bending. The arc length is kept constant as the central axis of the bellow is assumed to have a constant length. This length can be used to calculate the major radius of the torus. The minor radius of the torus is assumed to be constant. The major and minor radius, as well as the required angles are displayed in figure 10.

The poloidal (ϕ) and toroidal (θ) angles, along with the aforementioned major and minor radii, lead to the following coordinate equations:

$$\mathbf{u}_i = \begin{bmatrix} x_i \\ y_i \\ z_i \end{bmatrix} = \begin{bmatrix} (L_i + l_i \cos(\phi_i)) \cos(\theta_i) - L_i \\ l_i \sin(\phi_i) \\ (L_i + l_i \cos(\phi_i)) \sin(\theta_i) \end{bmatrix} \tag{1}$$

Where $\mathbf{u}_i$ indicate the position vectors for the rods, L is the major radius, l is the minor radius. ϕ is the poloidal angle ($-180° \leq \phi \leq 180°$) , and θ is the toroidal angle ($0° \leq \theta \leq \theta_{max}$, where θ_{max} is the bending angle of the bellow). By subtracting L in equation 1, the base of the section of the torus is placed at the origin.

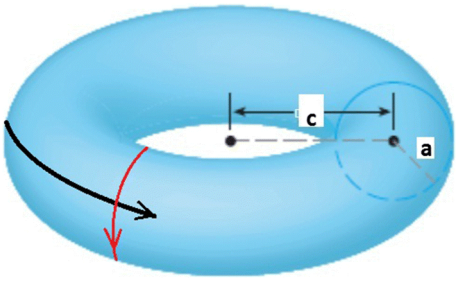

Figure 10: The required torus distances and angles [13]. The red arrow indicates the poloidal angle (ϕ) and the leftmost black arrow indicates the toroidal angle (θ). c indicates the major radius, and a the minor radius.

These equations are used for both bellows. To rotate the rod and thus visualising the bellow bending in another direction than towards the x-axis, rotation matrices must be used. These are as follows:

$$R_z = \begin{bmatrix} \cos(\alpha_i) & -\sin(\alpha_i) & 0 \\ \sin(\alpha_i) & \cos(\alpha_i) & 0 \\ 0 & 0 & 1 \end{bmatrix} \tag{2}$$

$$R_y = \begin{bmatrix} \cos(\beta) & 0 & \sin(\beta) \\ 0 & 1 & 0 \\ -\sin(\beta) & 0 & \cos(\beta) \end{bmatrix} \tag{3}$$

Where R_z is the rotation matrix around the z-axis, one of which is require for each bellow, α_i is the rotation around the z-axis, and β is the rotation around around the y-axis, which is only required for the second rod to align its base to the top of the first rod. To then align transform the base of the second rod to the top of the first rod, the coordinates of the center of the top of the first rod must be found:

$$\mathbf{c} = \begin{bmatrix} x_c \\ y_c \\ z_c \end{bmatrix} = \begin{bmatrix} d\sin(\gamma)\cos(\alpha) \\ d\sin(\gamma)\cos(\alpha) \\ d\cos(\alpha) \end{bmatrix}, \gamma = 90° - \frac{180° - \theta_{max}}{2} \tag{4}$$

$$2L\sin(\theta_{max}/2) \tag{5}$$

Where x_c,y_c, and z_c are the center coordinates for the top of the first rod, d equals the chord length, and γ is the angle between the z-axis and the chord. The coordinates of the points on the rotated rods are then given by:

$$\mathbf{u}_r^1 = \mathbf{R}_z^1 \left(\mathbf{R}_b \mathbf{u}_1\right) \tag{6}$$

$$\mathbf{u}_r^2 = \mathbf{R}_z^1 \left(\mathbf{R}_y^2 \mathbf{R}_z^2 \mathbf{R}_b \mathbf{u}_2\right) + \mathbf{c} \tag{7}$$

Where $\mathbf{u}_r^1$ and $\mathbf{u}_r^2$ are the position vectors for each point on the first rod and second rod respectively, and $\mathbf{R}_b$ is a base z-rotation that eliminates the 180°offset. The resulting avatar can be seen in figure 11.

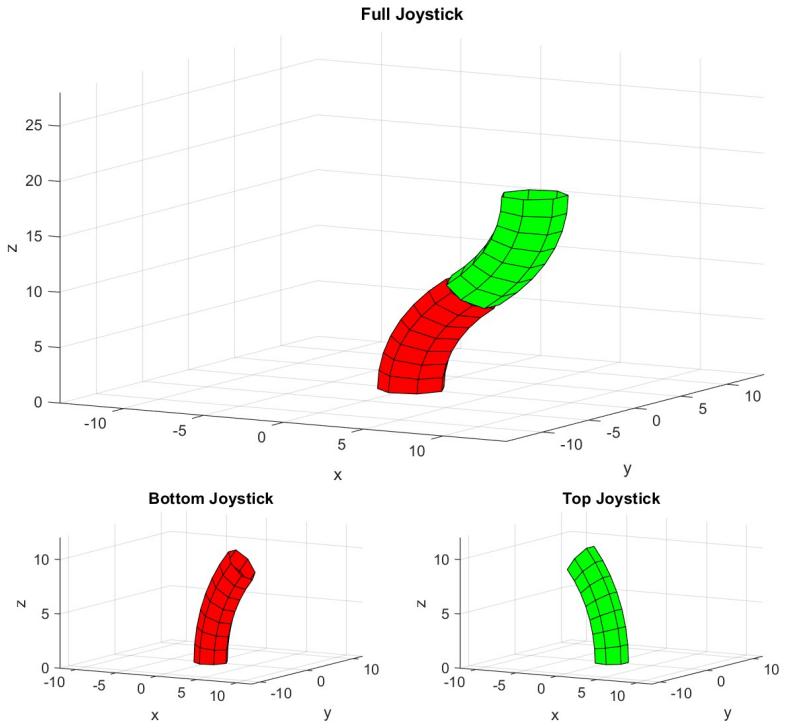

Figure 11 The digital avatar of the joystick. $\alpha_1 = 0\,\mathrm{deg}, \alpha_2 = 180°$. $\theta_{max,1} = \theta_{max,2} = 45°$

2.6 Data Acquisition and Processing

In order to acquire data from the piezoresistive CTPUC sensors to use as input for the avatar, the joystick's sensors still need to be connected digitally. As such, they are connected to an Arduino Nano (Arduino, Italy) along with a 16 channel Multiplexer (SparkFun Electronics, USA) and a 16-bit Analog to Digital Converter (ADC) (Seeedstudio, China). A wiring schematic is given in figure 12. The Arduino gives a 5V output, which goes through a resistor before being directed by the Multiplexer. At the node between the resistor and the multiplexer, the circuit is wired to the ADC board, which measures the voltage over the node in 16-bit ADC. The 16-bit allows for a high data resolution, likewise leading to a high resistance resolution. The ADC is also connected to the Arduino using Inter-Integrated Circuit (I^2C), and an Arduino library was downloaded to interface the two components. The sensor data is sent over USB to a computer for processing.

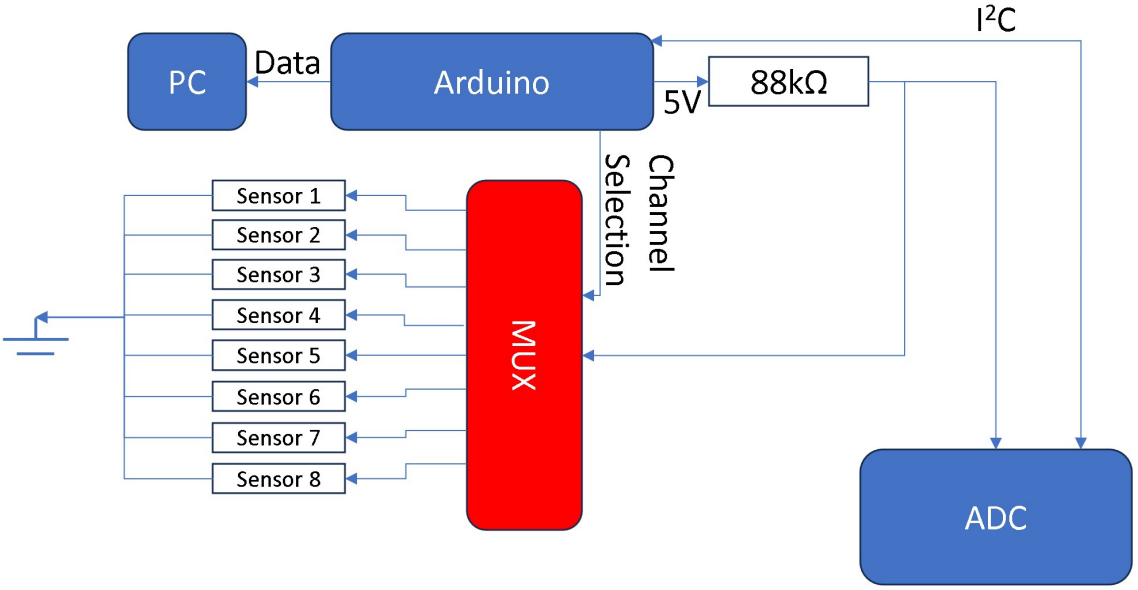

Figure 12 A schematic representation of the wiring setup.

For the bottom bellow, copper wires are attached at the bottom to the CTPUC. At the top of that bellow, the CTPUC connects in a central groove at the end surface (see figure 13), which is connected to ground by wire. This is mirrored in the top bellow. To ensure proper connection between the ground connections of both bellows, copper tape is applied on one of the bellows.

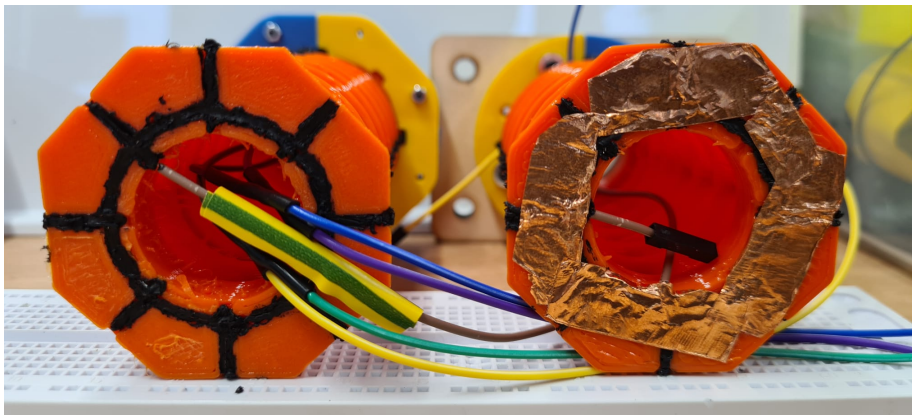

Figure 13 The connecting surfaces between the top (left) and bottom (right) bellows.

Gathering the sensor data was done by measuring their response to manual bending of the joystick. The following tests were performed for each half-joystick separately:

1. Bending once to 90 degrees in one direction, then the opposite direction.
   This test serves to study the response of opposite sensors to stretching and subsequent compression of the bellow and sensor geometry.

2. Bending the bellow to 90 degrees, then rotating the bellow once counterclockwise.
   This tests the consistency or inconsistency of the sensors as a response to subsequent similar manipulation, as well as the response of the sensors to movement other than straight away or towards it.

3. Bending once in one direction, then returning it to base position.
   This test serves to discover the back-to-baseline time for the sensor.

4. for each axis: repeated bending.
   This serves to test the consistency of the sensor response with repeated consistent manipulation.

For the complete combined joystick the tests that were performed were mainly to study the behaviour of the joystick in its entirety and to check for unwanted disturbances the sensors of the two halves of the joystick could have on each other. These tests are as follows:

1. Bend the bellow into an S-shape

2. Bend the bellow into a C-shape

After acquiring the measurement data, it was analysed in MATLAB. To study the data as resistance rather than voltage, which is the charactertic changing quality of the piezoresistive CTPUC, the following formula was used.

$$R_p = \frac{R_1}{V_s - V_i} V_i \tag{8}$$

This equation is derived from the equation of a voltage divider. R_p equals the sensor resistance, R_1 equals the resistor's resistance, V_s is the Arduino's source 5V, and V_i is the i'th sensor's voltage output. After normalising the data by their stable starting values and calculating the resulting extremes, resistance intervals were calculated which were used to roughly estimate the joystick's angle and orientation. This data is then used as input for the avatar, completing the joystick-avatar interface.

3 Results and Discussion

3.1 Physical Joystick

The fabrication of physical components of the joystick was successful (see figure 14a). Both bellows were able to be printed and connected using the connection pieces (see figure 14b). The application of the CTPUC was successful as well, though in some spots extra material had to be added by hand, and during testing some discontinuities in the corrugation dips had to be repaired (see figure 14c), which resulted the presence of higher volumes and a wider section of material being present in the bottom right and bottom left sensors especially. In final assembly, each bellow could bent to approximately 90°(see figure 14d. There are still some issues with the print of the bellow including stringing and warping, which can be be seen in appendix A along with previous attempts at printing the conductive CTPUC.

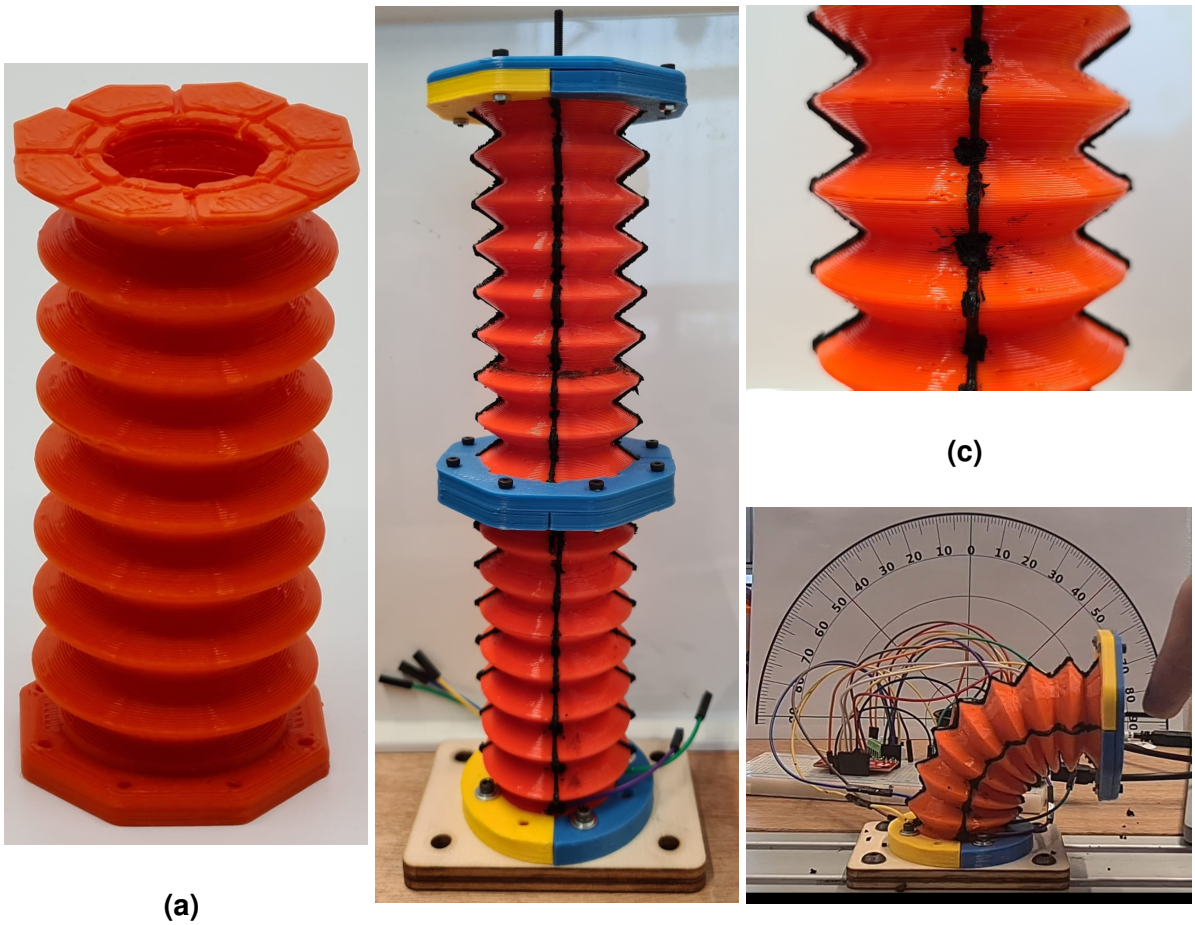

(a) **(b)** **(c)** **(d)**

Figure 14: (a): The bottom bellow before application of the CTPUC. (b): The final assembly of the joystick. (c): The repaired discontinuity in the corrugation dips. (d): A demonstration of the bending angle of the bottom bellow and the experimental setup for the testing of the bottom bellow.

3.2 Sensor Resistance Data

The experiments were performed in the setup in figure 15. The sensors are indicated in the blocks, the colours of which coincide with the colours of the plots in the graphs. For prefix ”B” is used for the bottom bellow, and ”T” for the top bellow. For the experiments, resulting figures were chosen that best highlighted certain characteristics or patterns. Additional figures can be found in appendix B.

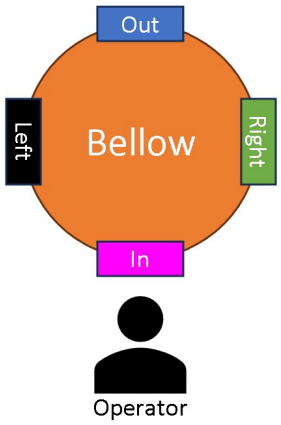

Figure 15 A schematic overview of the experimental setup.

In the tests that were performed, results were inconsistent in numerical values between sensors as can be seen in figure 16, which displays the resistances plots of the experiments where the bellow is first bent to the right, then turned counterclockwise one rotation. However, clear patterns and behavioural consistencies can be observed in the plots of both halves of the joystick. There is a measurable response both when the bellow is bent away from the sensor and when it is bent towards the sensor. The signals for bending towards and bending away are however very different. Bending away gives a sharp peak of high amplitude (bottom left and bottom right sensors, figure 16a), or elevations with secondary peaks (top bellow sensor, figure 16b). The dips indicating the bellow moving towards the sensor generally have a smaller change in resistance, though they appear relatively smooth. Furthermore, for each sensor there appears to be some oscillating behaviour in the steady states at the start and end when no manipulation is applied. There also appears to be a difference in resistance in these steady states, with the steady state at the end of the experiment having a markedly lower resistance than that at the start.

The discrepancy in absolute values of the sensors are likely to be attributable to the inconsistencies in CTPUC printing dimensions and (specifically for the bottom left and right sensors) to the repairs made to discontinuities. These repairs caused there to be more material in the corrugation dips, increasing the potential amount of interacting CTPUC. Why this has also lead to the greater increase in resistance is uncertain, but it could be due to the repair quality, possibly introducing small discontinuities.

The resistance profiles of the sensors can be explained with a combination of phenomena. For bending away from the sensor, this comes down to a combination the piezoresistive [14] and viscoelastic [15] properties of the material. The resulting signals when bending away from

the sensor are choppy and contain expected though unwanted secondary peaks. The resistance dips resulting from the bellow bending towards the sensor were in general far smoother than the resistance peaks when the bellow was bent away. These dips are caused in part by compression and in part by in part by an increased number of contact points resulting in shorter current pathways. The relatively low amount of unwanted artifacts in the resistance dips are important observation, as they suggests the resistance data for the joystick bending towards the sensor is potentially considerably more valuable than the resistance data resulting from the joystick moving away from the sensor. The changes in steady state values, while undesirable, have previously been documented [16] and were therefore expected.

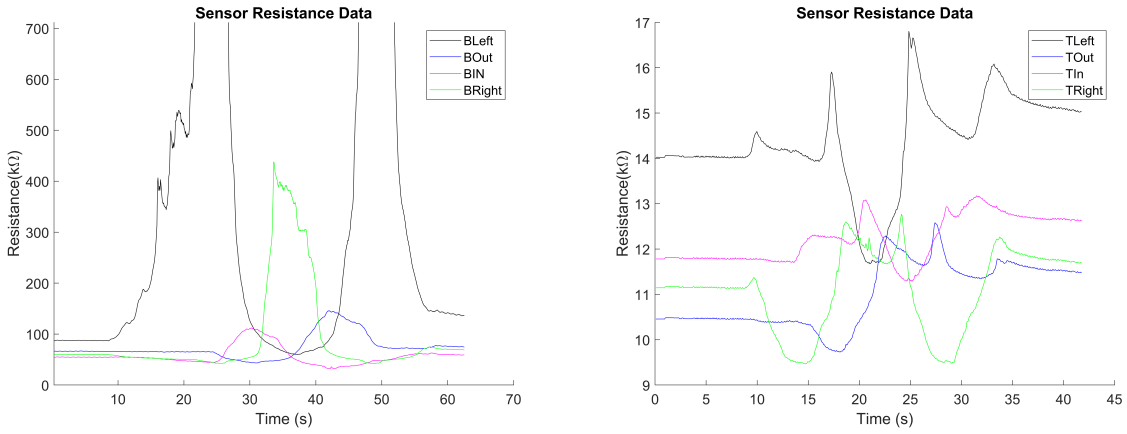

(a) **(b)**

Figure 16: Resulting resistance plots from the bend right then circle counterclockwise experiments. (a): bottom bellow, (b): top bellow.

Looking at the plots of the repeated movement in a single direction (see figure 17), the resistance change in the sensor the bellow is bent away from is relatively high compared to that of the sensor the bellow is bent towards. Furthermore, the bottom outward sensor seems to experience some disturbance from the movement, while the bottom inward sensor appears relatively constant. For the top bellow, the resistance dips in the sensor in the direction of the bending seem similar to the resistance peaks of the sensor in the other direction. The top left and right sensor seem to have some influence on each other as well, judging by their similar peak heights per repetition.

The reason for the disturbance in the bottom outer sensor is uncertain, though it could be attributed either to sideways bending of the sensor having some effect on the resistance, or possibly to artifacts caused by the sensors being interconnected at the electrical ground at one end of the bellow. These artifacts might also explain the similar peak heights of the opposing sensors in the top bellow. Why the bottom inward sensor does not share the same disturbance is unknown.

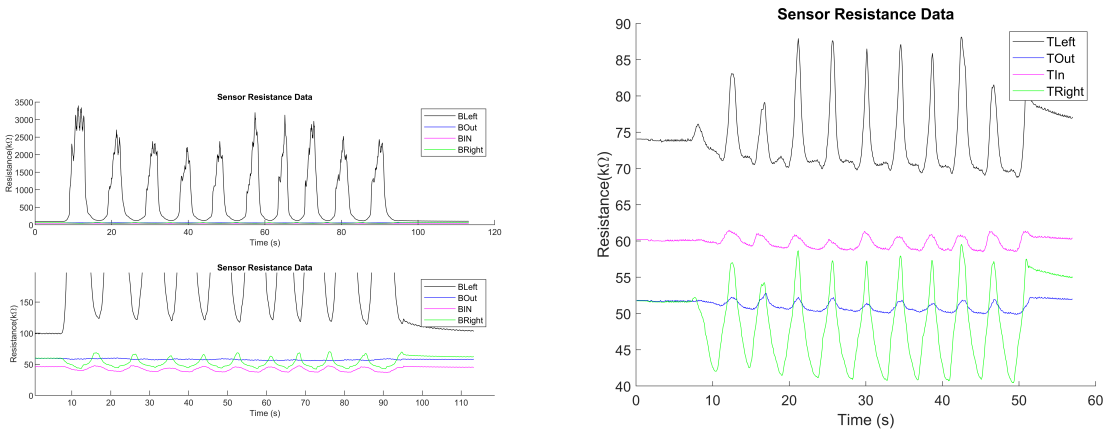

(a) **(b)**

Figure 17: Resulting resistance plots the repeated bends to the right. a: bottom bellow b: top bellow

Some of the sensors exhibit consistent patterns in their resistance peak profiles. When looking at figure 18, several features stand out. The peaks of the signal seem to contain two secondary peaks, one when the bellow is bent and one when it is returned. Between these secondary peaks, there is a gradual decrease in resistance. These features are most prominent in figure 18a, but can be recognised in figure 18b, indicating that this behaviour is consistent over different sensors. In both plots, there is a noticeable recovery overshoot when the bellow is returned to its original position.

The resistance peak profiles observed in these sensors have been previously observed when working with this material [17], including the recovery peaks [18], and while they are unwanted artifacts in these sensors, they were expected. Why this behaviour is seen more strongly in some sensors than in others is unknown, but it could be the result of instabilities in the operator's hand when performing the experiments, which could have amplified or weakened some of these features.

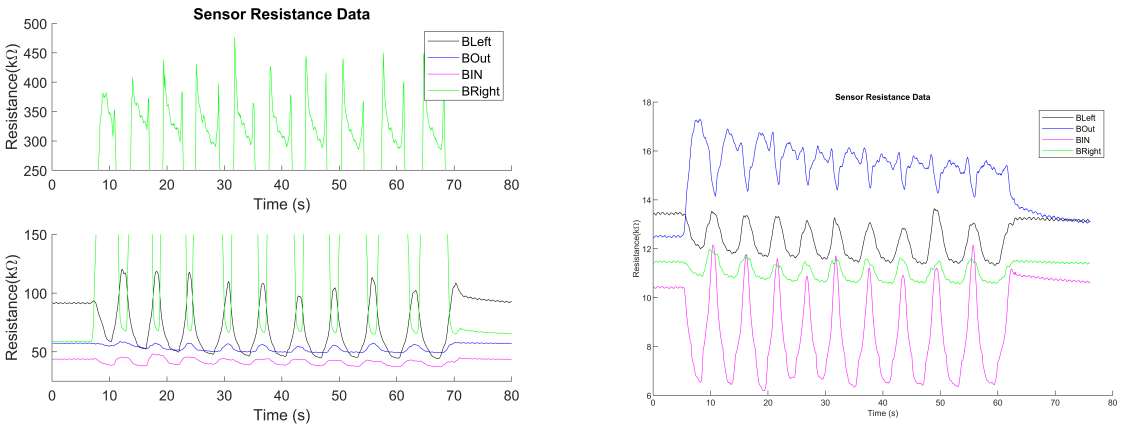

(a) **(b)**

Figure 18: Resulting resistance plots the repeated leftward and inward bends of the bottom bellow. a: leftward b: inward.

Some of the same traits observed in single bellow experiment can be observed in the full joystick experiments as well, as can be seen in the S-shape experiment in figure 19. Resistance patterns are consistent with what is expected, approximately following the bending profiles, however the signals vary greatly in strength and are not as easily recognisable as in previous experiments. There appear to be several profile features, such as previously observed elevation changes, secondary peaks, and signals seemingly influencing each other, though they are more prominent than in those experiments.

In both the S- and C-shape experiment, another observation can be made about the behaviour of the bottom left sensor (see figure 20). When the bellow is bent away from that sensor, the signal shows a sharp increase in resistance before oscillating around a plateau at a high resistance value compared to the other sensor values.

The resistance signal attributes in the combined joystick are clearly not as clear or easily readable as those of the single bellows. While the patterns attributed to material properties will not have changed, it is possible that the effect of operator inaccuracies may have increased due to handling the entire joystick at once. It is likely that the strong increase in resistance and oscillating plateau behaviour in the peak of the bottom left sensor can be attributed to a new CTPUC discontinuity, as these strong oscillations have previously been observed in the experimental setup when one of the bellows was not connected.

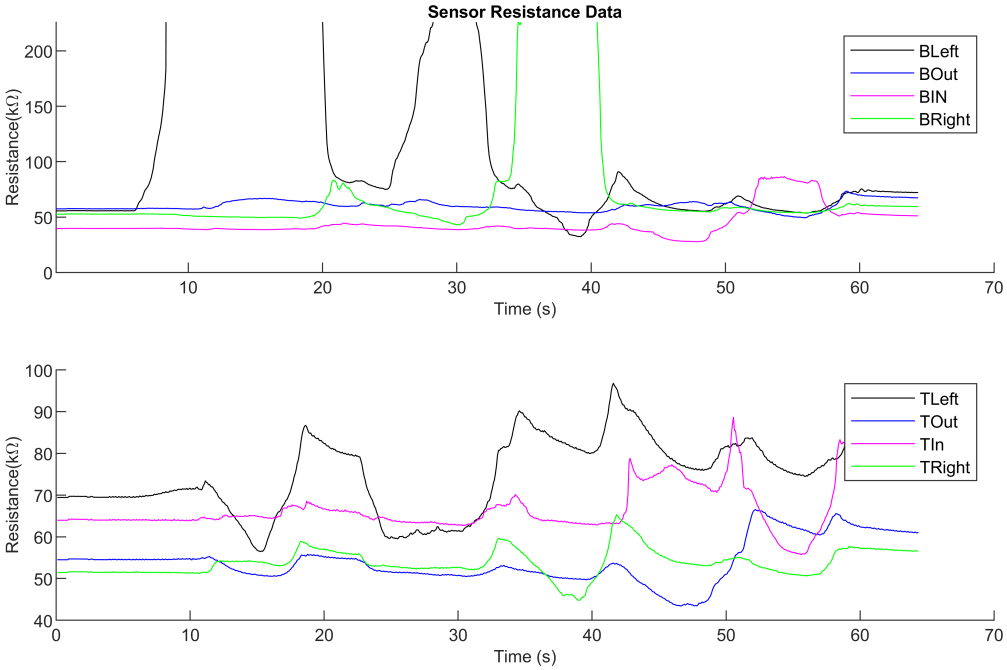

Figure 19: The resistance plots for the combined bellows in the S-shape experiment. The top plot is the bottom bellow, and the bottom plot is the top bellow. The order of bending for the bottom bellow was right twice, then once left, then once inward, then once outward. For the top bellow, the directions were all directly opposite.

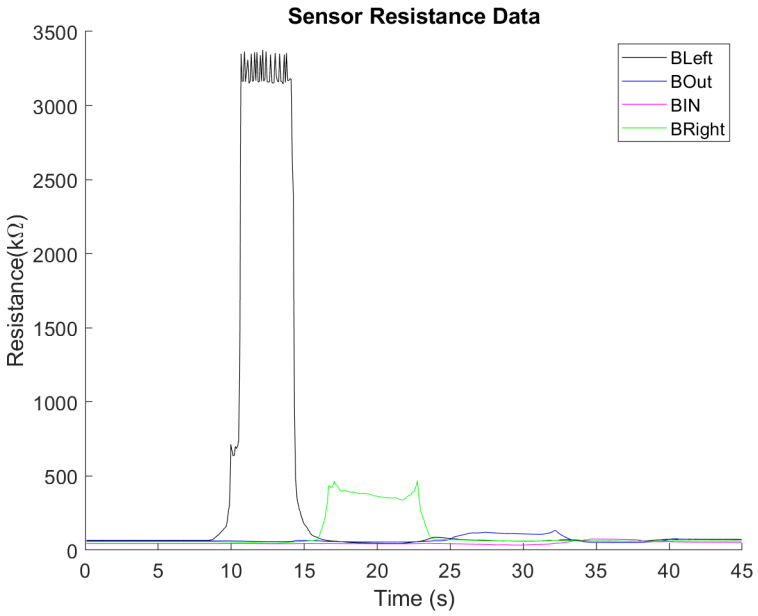

Figure 20 The resistance plots for the bottom bellow in the C-shape experiment.

For the C-Shape experiment, the signal profiles previously observed are not as clear in the top bellow but appear strongly in the bottom bellow, as can be seen in figure 21. In the bottom bellow, dips and peaks appear where expected, and few unexpected profile features

are present. On the top bellow, however, the profile features are not as clear. While dips and peaks appear mostly where expected, there are more unwanted profile features present such as the instability of the top inward signal in the first 25 seconds and its high extra peaks at the start and end of its expected peak.

The reason the signal profiles in the this experiment are less clear than in previously mentioned experiments is unknown. It is important to note, however, that this signal is still quite readily usable to interface with the avatar, as will be discussed in section 3.3.

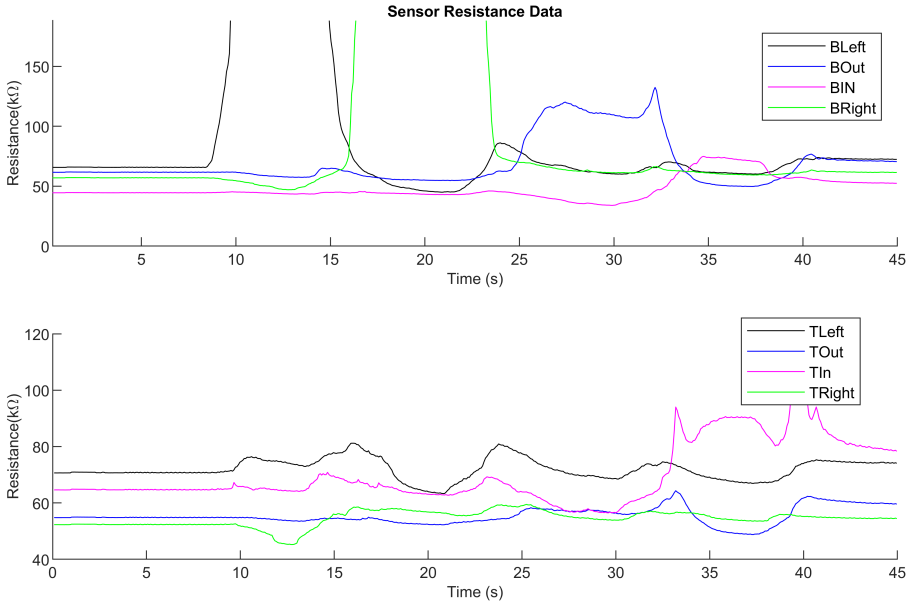

Figure 21: The resistance plots for the combined bellows in the C-shape experiment. The top plot is the bottom bellow, and the bottom plot is the top bellow. The order of bending for both bellows are to the right, then left, the inward, then outward.

3.3 Avatar Interface

The angle data for the avatar was derived from the sensor data by normalising (subtracting) the data sets by their baseline starting value, subtracting the opposing sensor values from each other, and using the extrema of those values to create 10 resistance intervals which would be assigned an angle. The orientation was calculated using the atan2 function and the bending angle was simply the highest bending angle of the two bending directions. An example of this for a single bellow can be seen in figure 22. While the refresh rate of the avatar and angle resolution are low, it recognisably follows the movement of the bellow as it was manipulated.

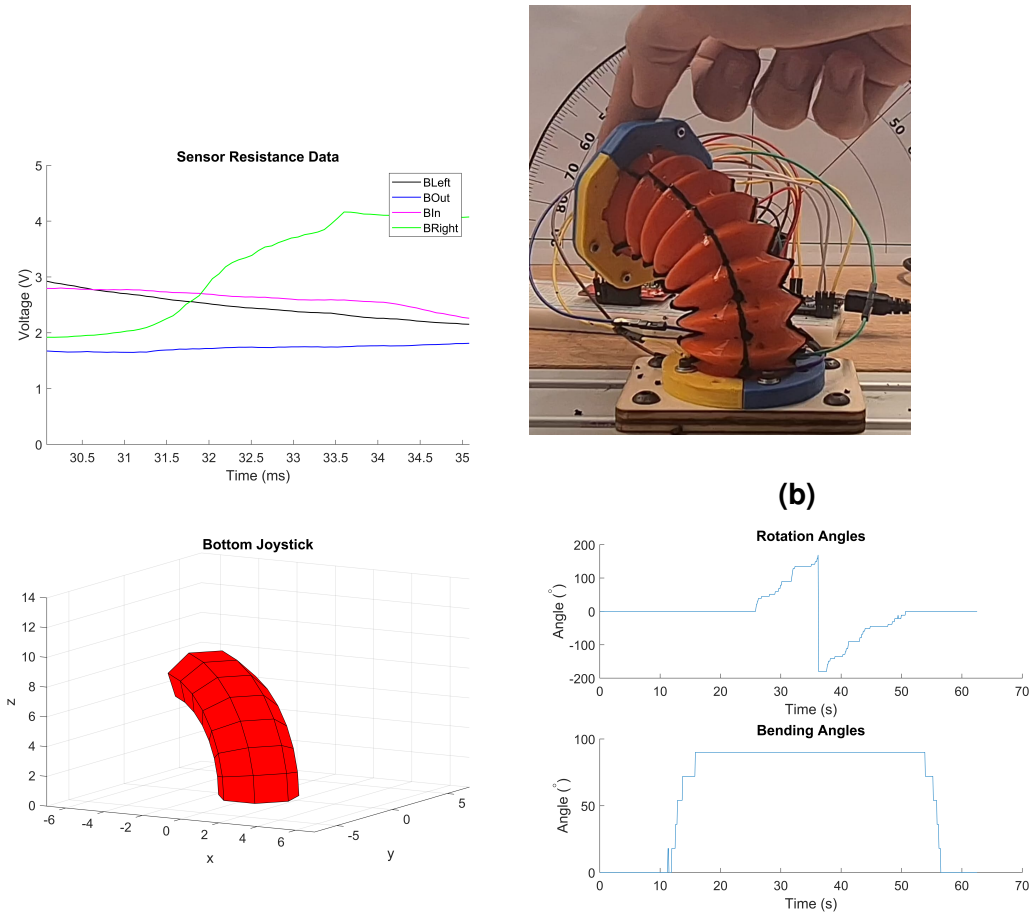

Figure 22: (a): a snapshot of the current resistance measurement and the corresponding avatar configuration. (b): a snapshot of the joystick, which is interfaced with the avatar. (c): the bending and rotation angles over the duration of the experiment.

When interfacing the complete joystick with the avatar, the angle pattern was not as clear as it was for the single bellow, as can be seen in figure 23c. Nevertheless, the avatar still recognisably follows the manipulation pattern. Unfortunately, the results for the S-shape experiment were not as clear, as can be seen in figure 24. Some of the expected movement patterns can still be recognised in the plot, but in general the C-shape experiments gave far clearer results.

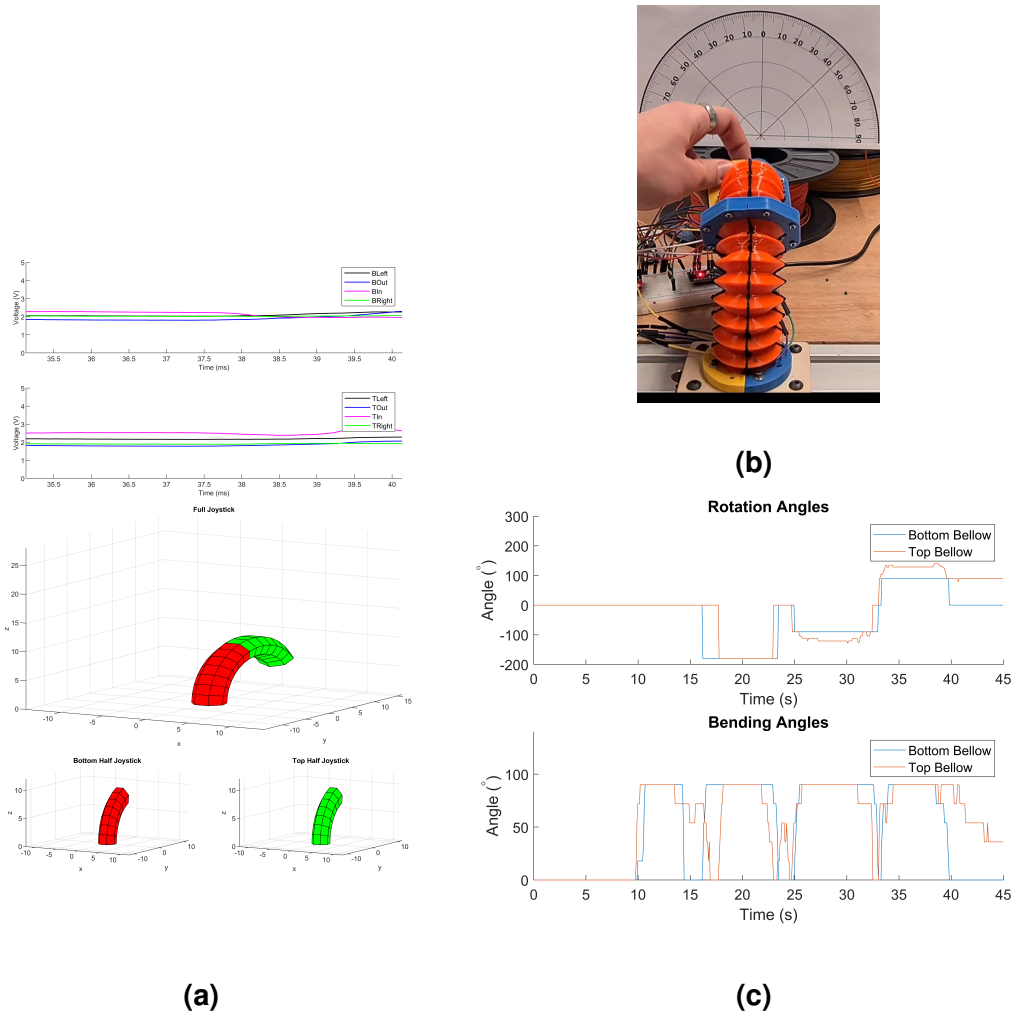

Figure 23: (a): a snapshot of the current resistance measurement and the corresponding avatar configuration. (b): a snapshot of the joystick, which is interfaced with the avatar. (c): the bending and rotation angles over the duration of the experiment.

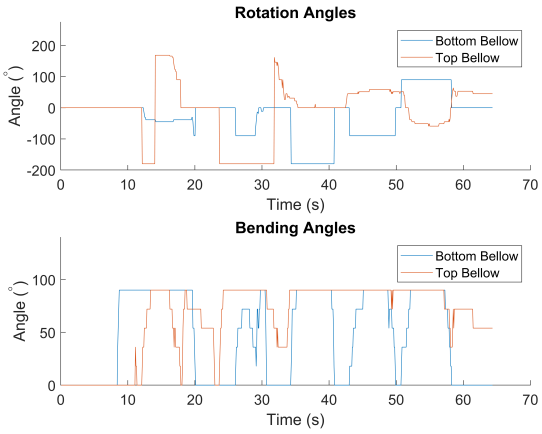

Figure 24 The angle plot for the S-shape experiment.

3.4 Validation

To validate that the resistance intervals were consistent across experiments, the intervals of the bottom bellow bending and rotating around the z-axis were applied to the sensor data of the repeated bending experiments of the bottom bellow, which provided the results in figure 25. Each of these figures show repeated bending in the direction which was expected. In the repeated outward bending, however, the rotation angle seems to plateau in the last few repetitions, which is inconsistent with the movement pattern. Furthermore, the angle changes appear to be more acute than is expected from the manipulation pattern.

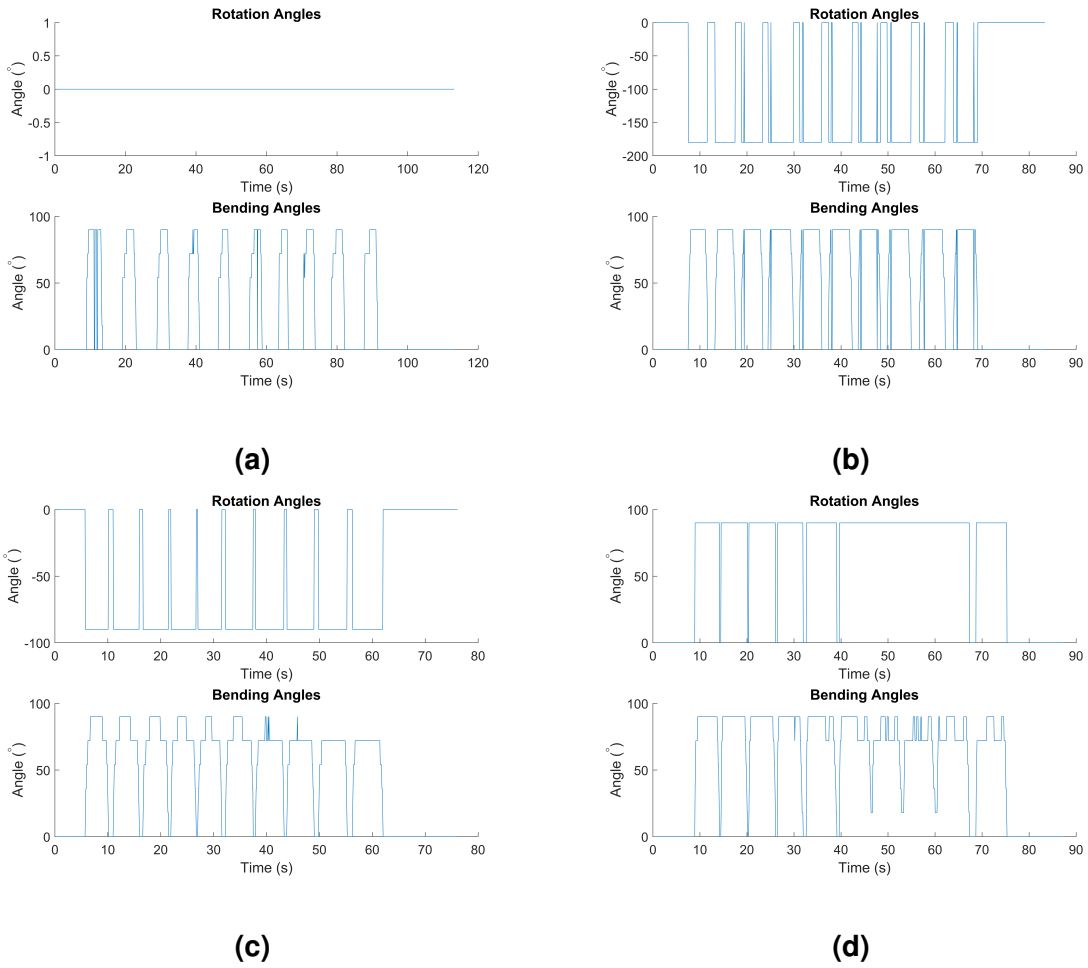

Figure 25: The bending angle data of for repeated bending experiments using the risistance thresholds from bend-then-circle experiment. (a):repeated rightwards bends , (b): repeated leftwards bends, (c): repeated inward bends. (d): repeated outward bends.

4 Conclusions

4.1 Joystick

This thesis shows the feasibility and potential of 3-D printing haptic teleoperation controllers for use in continuously manipulable soft robotics. While the 3-D printing of the CTPUC still requires improvement, the possibility of directly printing sensor material on the joystick provides a promising prospect for the future of cost effective, easy to produce haptic control hardware. There are still some challenges to be overcome, like the printing errors in the bellow printing and the inconsistencies in sensor printing quality and dimensions.

4.2 Sensor Data and Avatar Interface

The experiments that were performed proved that the CTPUC sensors were usable for interfacing the joystick's movement with the digital avatar. However, the acquired data was far from consistent and contained resistance profile features which made it difficult to accurately reconstruct the joystick's angular data accurately and consistently. Furthermore, there seems to be greater promise in using the resistance dips rather than the resistance peaks. The sensor setup on the joystick also does not provide the possibility to fully derive the infinite degree of freedom orientation and bending profile of the joystick. To that end, other sensor and/or circuit setups must be constructed. Regardless, the possibility to recognisably reconstruct the movement of the joystick with the simple calculations used to turn the resistance values into angle intervals for the avatar shows the great potential of these sensors.

4.3 Recommendations

The main focus of future iterations of the joystick should be the improvement of the sensors. While the printing of the CTPUC creates a very straight line over the bellow, the thickness and adhesion could be improved by using a better geometry analysis method to consistently apply the sensor material, and a custom sharper and longer nozzle would help in better reaching the geometries in the corrugations. Furthermore, for printing the bellows themselves, using a direct drive printing head rather than the default one of the used printer could significantly improve the print quality by reducing the need for extra flow and reduced retraction.

In terms of the sensors and their data, more trials must be done using varying parameters for the sensor printing, including sensor line width and thickness. This may improve the sensor quality and consistency. Furthermore, since the resistance dips gave smoother plots than the peaks, it would likely be fruitful to experiment with using just those parts of the signal, compensating for the drift in baseline resistance. Furthermore, while these simple angle derivations worked fine for a proof of concept, the signals should be further studied to achieve more accurate angle data for the joystick. Finally, other sensor setups must be constructed to allow for true continuous geometry sensing, which this joystick does not yet allow.

References

[1] O. Yasa, Y. Toshimitsu, M. Y. Michelis, L. S. Jones, M. Filippi, T. Buchner, and R. K. Katzschmann, "An overview of soft robotics," *Annual Review of Control, Robotics, and Autonomous Systems*, vol. 6, pp. 1–29, 2023.

[2] A. Sadeghi, A. Mondini, E. D. Dottore, A. K. Mishra, and B. Mazzolai, "Soft-legged wheel-based robot with terrestrial locomotion abilities," *Frontiers Robotics AI*, vol. 3, p. 223620, 2016.

[3] E. Brown, N. Rodenberg, J. Amend, A. Mozeika, E. Steltz, M. R. Zakin, H. Lipson, and H. M. Jaeger, "Universal robotic gripper based on the jamming of granular material," *Proceedings of the National Academy of Sciences of the United States of America*, vol. 107, pp. 18 809–18 814, 2010.

[4] J. E. Bernth, A. Arezzo, and H. Liu, "A novel robotic meshworm with segment-bending anchoring for colonoscopy," *IEEE Robotics and Automation Letters*, vol. 2, pp. 1718–1724, 2017.

[5] M. Runciman, A. Darzi, and G. P. Mylonas, "Soft robotics in minimally invasive surgery," *Soft Robotics*, vol. 6, pp. 423–443, 2019.

[6] C. Lee, M. Kim, Y. J. Kim, N. Hong, S. Ryu, H. J. Kim, and S. Kim, "Soft robot review," *International Journal of Control, Automation and Systems*, vol. 15, pp. 3–15, 2017.

[7] Unknown, "How endoscopes work," 2016, [Accessed 21-02-2024]. [Online]. Available: https://abdominalkey.com/how-endoscopes-work/

[8] J. Zhou, Y. Chen, X. Chen, Z. Wang, Y. Li, and Y. Liu, "A proprioceptive bellows (pb) actuator with position feedback and force estimation," *IEEE Robotics and Automation Letters*, vol. 5, pp. 1867–1874, 2020.

[9] A. Giri, R. Bloom, and T. K. Morimoto, "Hapstick: A soft flexible joystick for stiffness rendering via fiber jamming," *IEEE Robotics and Automation Letters*, vol. 8, pp. 4163–4170, 2023.

[10] NinjaTek, "Ninjaflex 3d printer filament (85a)," 2016, [Accessed 11-02-2024]. [Online]. Available: https://ninjatek.com/shop/ninjaflex/#tech-specs

[11] ——, "Eel 3d printer filament (90a)," 2016, [Accessed 11-02-2024]. [Online]. Available: https://ninjatek.com/shop/eel/#tech-specs

[12] Unknown, "Visualising a toroidal surface in matlab," 2012, [Accessed 03-01-2024]. [Online]. Available: https://stackoverflow.com/questions/10655393/visualizing-a-toroidal-surface-in-matlab

[13] S. Ghosh, "Geometric phases for classical and quantum dynamics: Hannay angle and berry phase for loops on a torus," *International Journal of Theoretical Physics 58(06):1-13*, 2019.

[14] K. Ke, V. S. Bonab, D. Yuan, and I. Manas-Zloczower, “Piezoresistive thermoplastic polyurethane nanocomposites with carbon nanostructures,” *Carbon*, vol. 139, pp. 52–58, 2018.

[15] H. Cho, S. Mayer, E. Pöselt, M. Susoff, P. J. Veld, G. C. Rutledge, and M. C. Boyce, “Deformation mechanisms of thermoplastic elastomers: Stress-strain behavior and constitutive modeling,” *Polymer*, vol. 128, pp. 87–99, 2017.

[16] Q. Chen, Q. Gao, X. Wang, D. W. Schubert, and X. Liu, “Flexible, conductive, and anisotropic thermoplastic polyurethane/polydopamine /mxene foam for piezoresistive sensors and motion monitoring,” *Composites Part A: Applied Science and Manufacturing*, vol. 155, p. 106838, 2022.

[17] A. Georgopoulou, T. Sebastian, and F. Clemens, “Thermoplastic elastomer composite filaments for strain sensing applications extruded with a fused deposition modelling 3d printer,” *Flexible and Printed Electronics*, vol. 5, p. 035002, 2020.

[18] S. Zheng, J. Deng, L. Yang, D. Ren, S. Huang, W. Yang, Z. Liu, and M. Yang, “Investigation on the piezoresistive behavior of high-density polyethylene/carbon black films in the elastic and plastic regimes,” *Composites Science and Technology*, vol. 97, pp. 34–40, 2014.

A Printing issues

As can be seen in figure 26, the interior of the bellows contain significant stringing. They are the result of high flow settings and low retraction as is standard for the chosen TPU [10], which were used to avoid under-extrusion during the print. The stringing do not appear on the outside of the bellow due to the printing path.

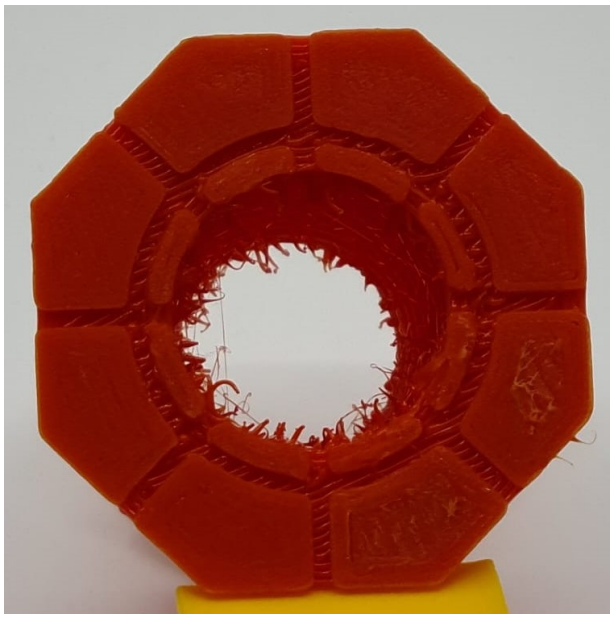

Figure 26: Stringing within the bellow structure, some of which was removed in post-processing.

Little bumps and crevices can be seen in parts of the bellow print in figure 27. The crevices especially weaken the structure of the bellow. The black material is a repair using TPU for layers which were under-extruded during the print. The colour is caused by remnants of CB, which proved difficult to purge from the hand printer but weren't enough to make the TPU conductive.

Figure 27 The top bellow, where some of the printing quality issues can be seen.

Figure 28 shows the result of the flexibility of the TPU during printing. The mismatch in figure 28b is the result of the wobble experienced during the print without using supports and attempting to manually stabilise the bellow during the print. The break and peeling of the initial layer in figure 28a are due to excessive bed adhesion, which made it difficult to remove the print from the printing surface.

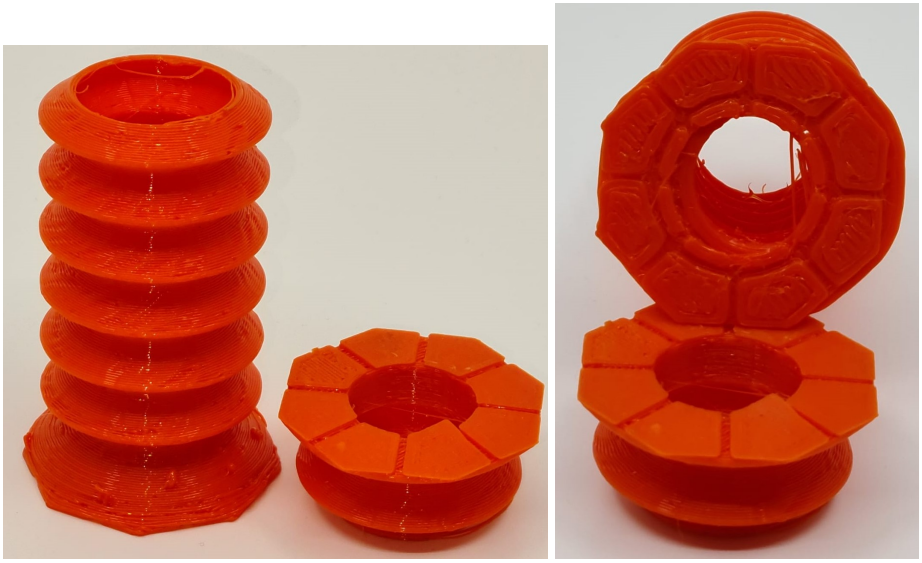

(a) **(b)**

Figure 28: Printing issues as a result of wobble and excessive bed adhesion. a: reakage and peeling of initial layer(s). b: breakage and layer mismatch.

B Extra Result Graphs

This appendix provides all resistance plots for the various experiments. This includes the graphs used in section 3. As mentioned in that section, the graphs that were chosen showed the most relevant results to discuss. However, for a full insight, the rest of the figures are provided here.

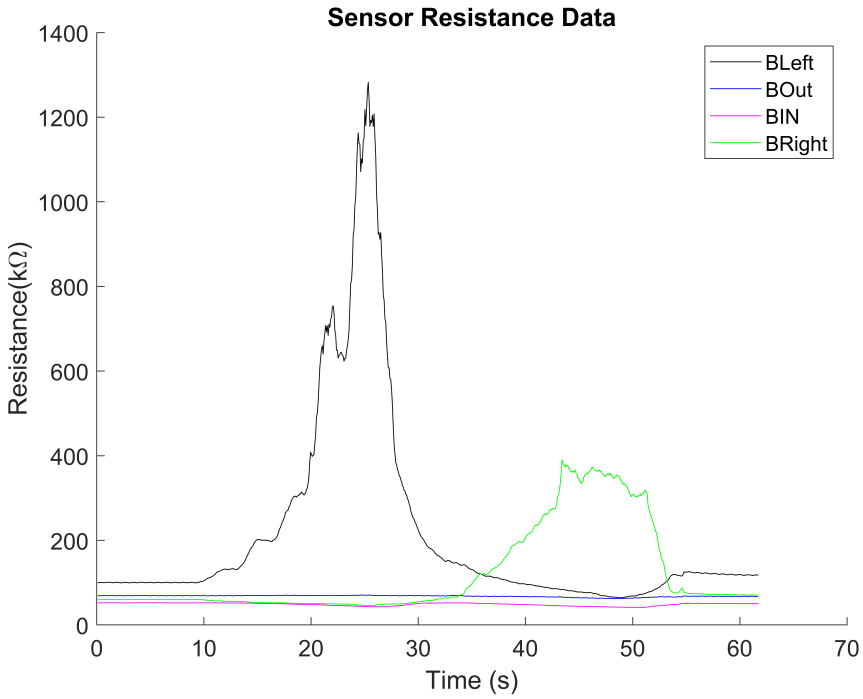

Figure 29 Resistance plot for bottom right then left bend

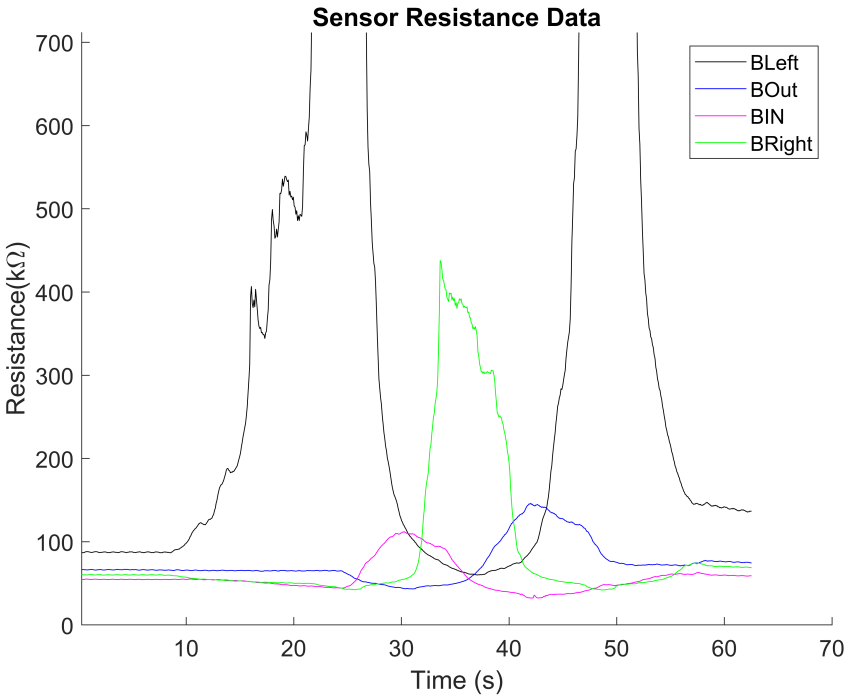

Figure 30 Resistance plot for bottom right the counterclockwise bend

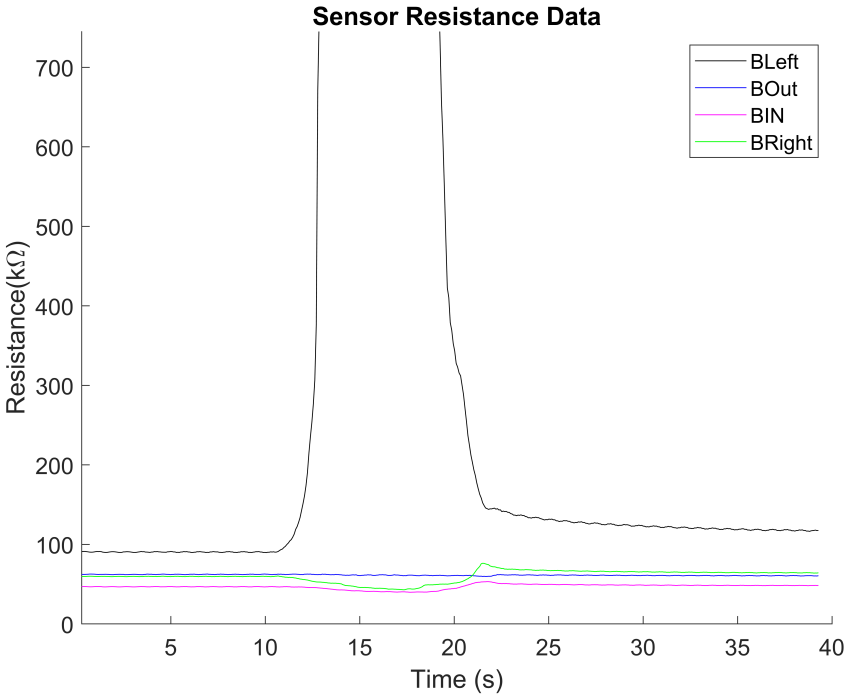

Figure 31 Resistance plot for bottom right bend then return

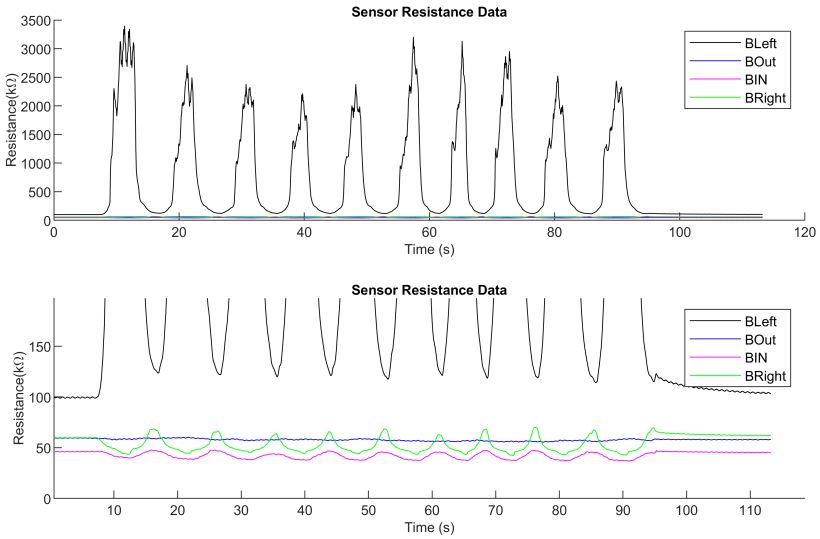

Figure 32 Resistance plot for the bottom right bend repeated

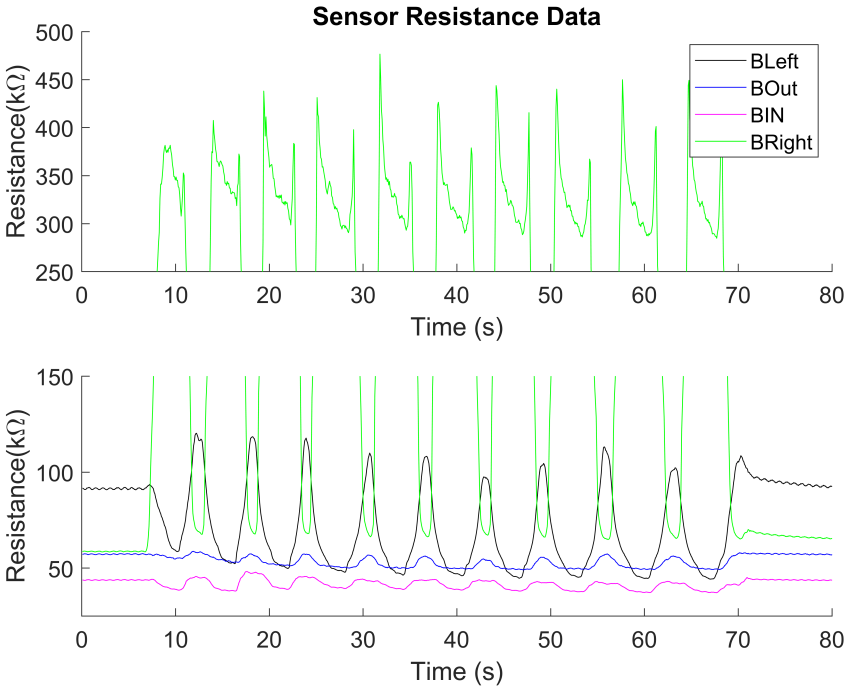

Figure 33 Resistance plot for the bottom left bend repeated

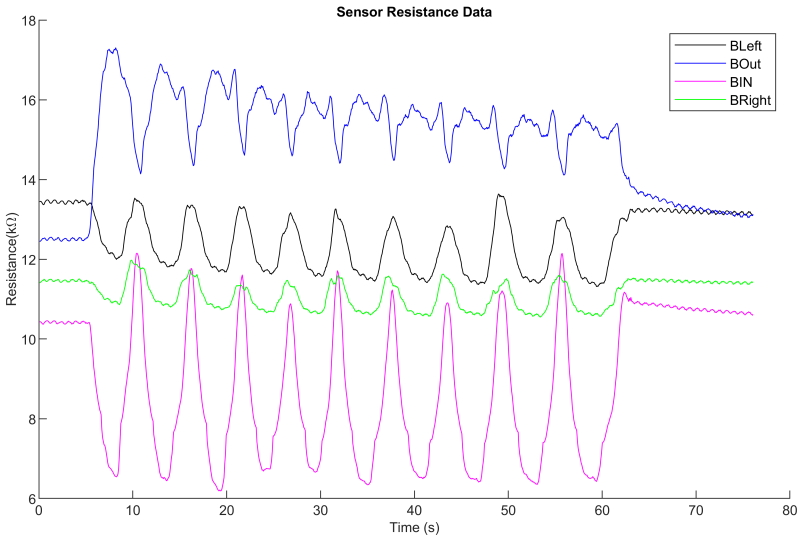

Figure 34 Resistance plot for the bottom inward bend repeated

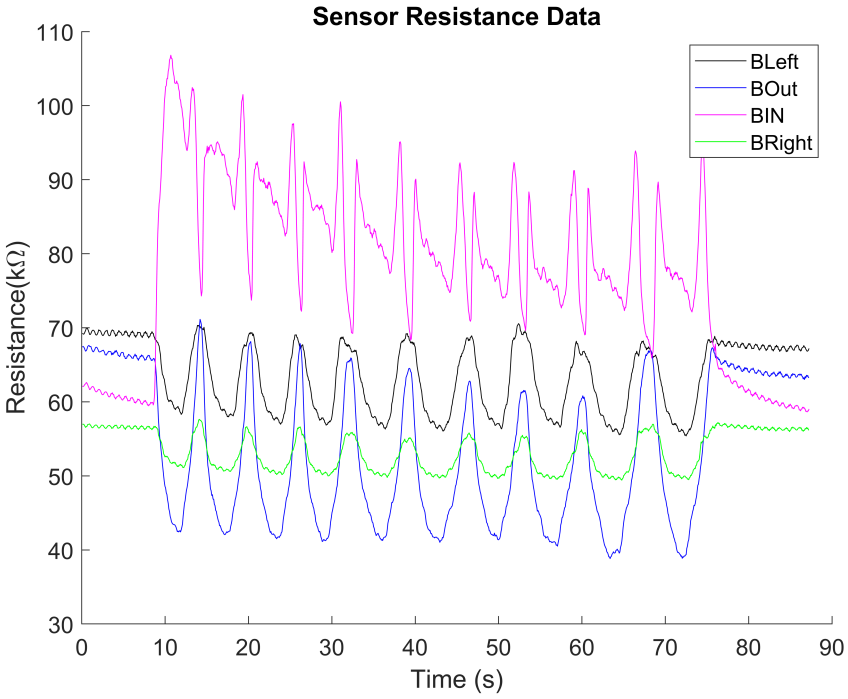

Figure 35 Resistance plot for the bottom outward bend repeated

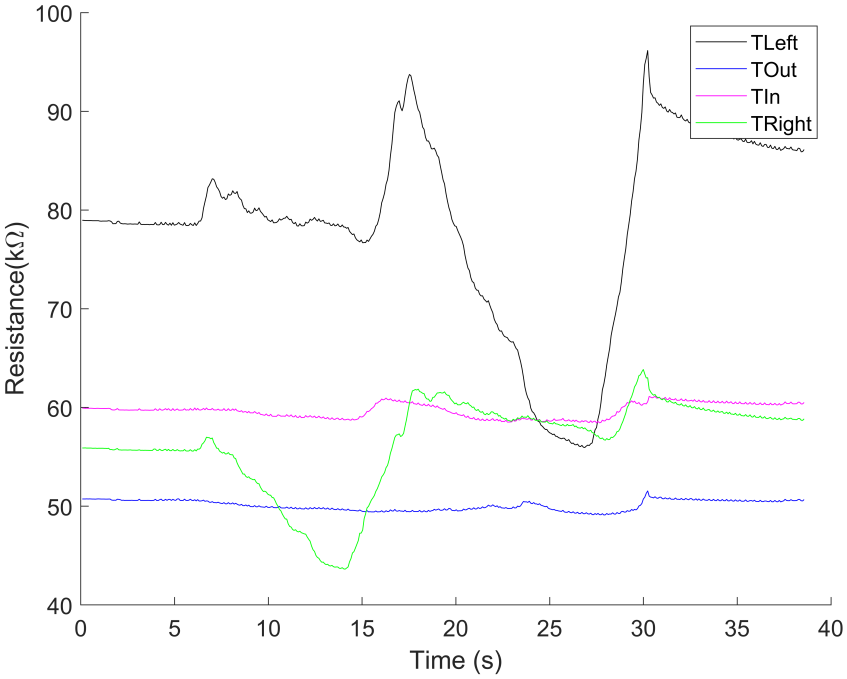

Figure 36 Resistance plot for the top right then left bend

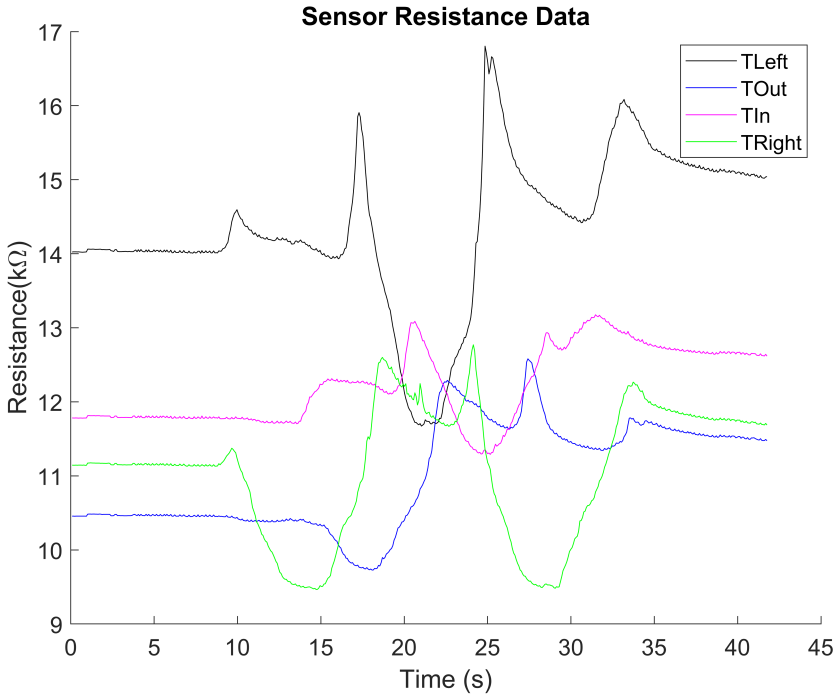

Figure 37 Resistance plot for the top right bend then circle counterclockwise

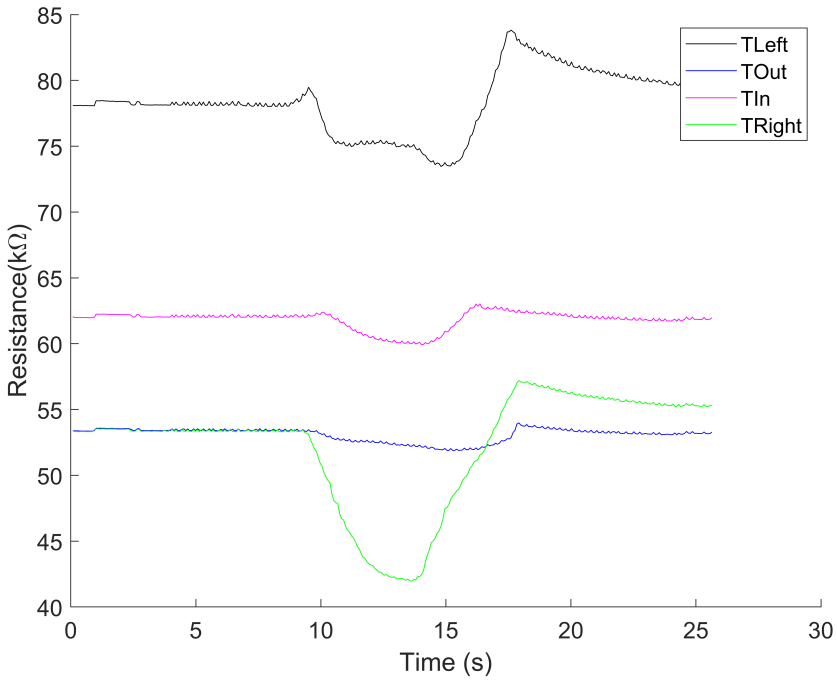

Figure 38 Resistance plot for the top right bend then return

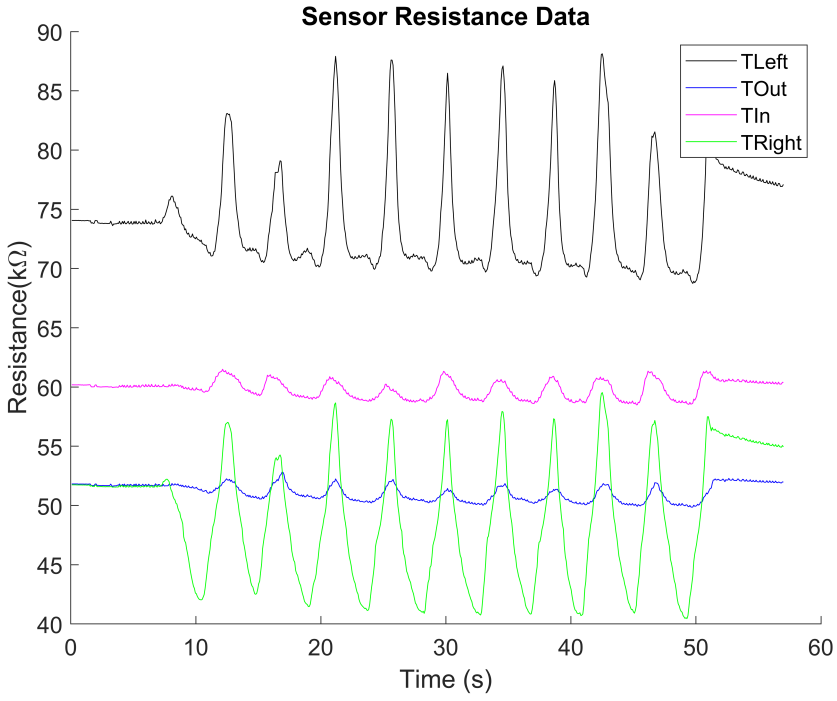

Figure 39 Resistance plot for the top right repeated bend

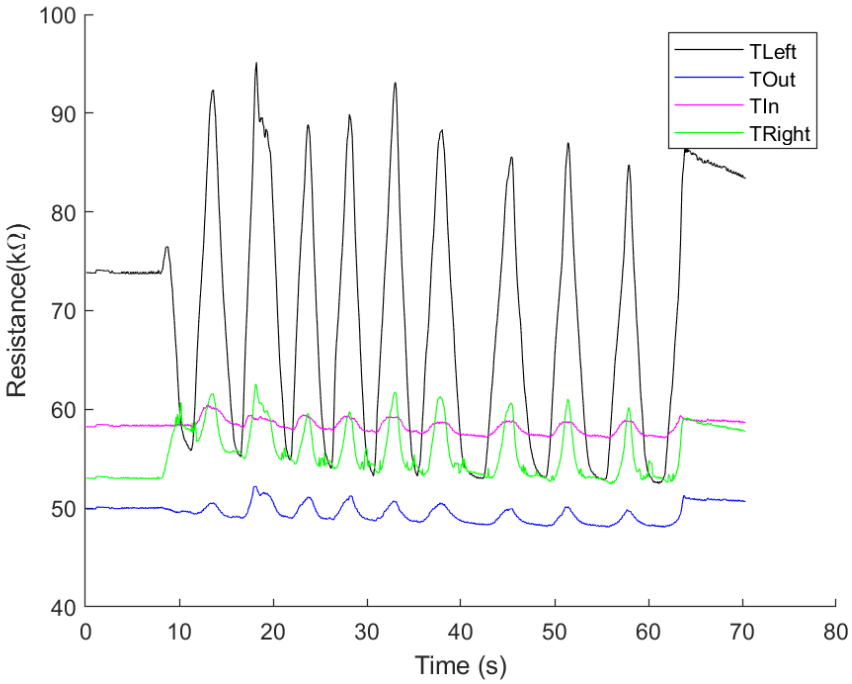

Figure 40 Resistance plot for the top left repeated bend

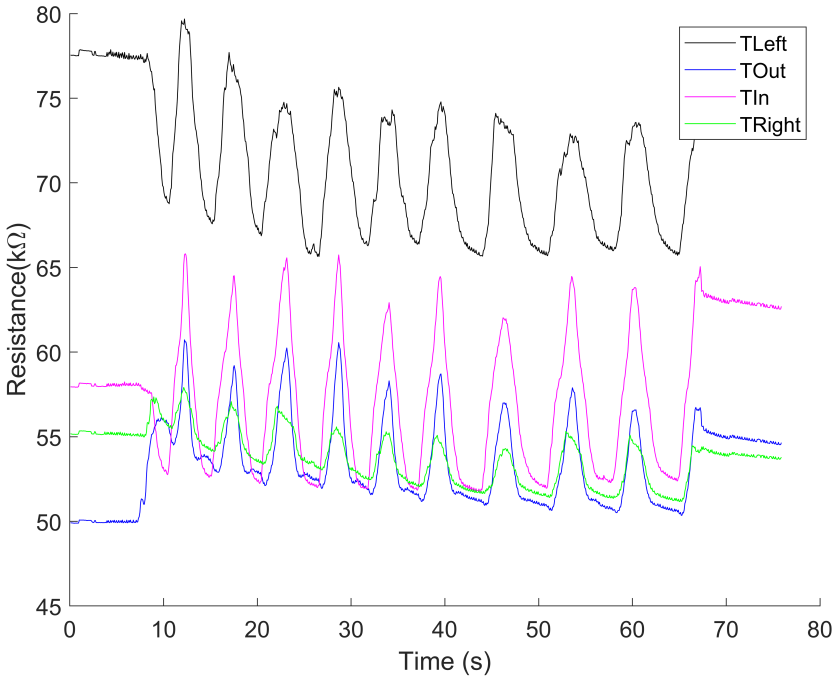

Figure 41 Resistance plot for the top inward repeated bend

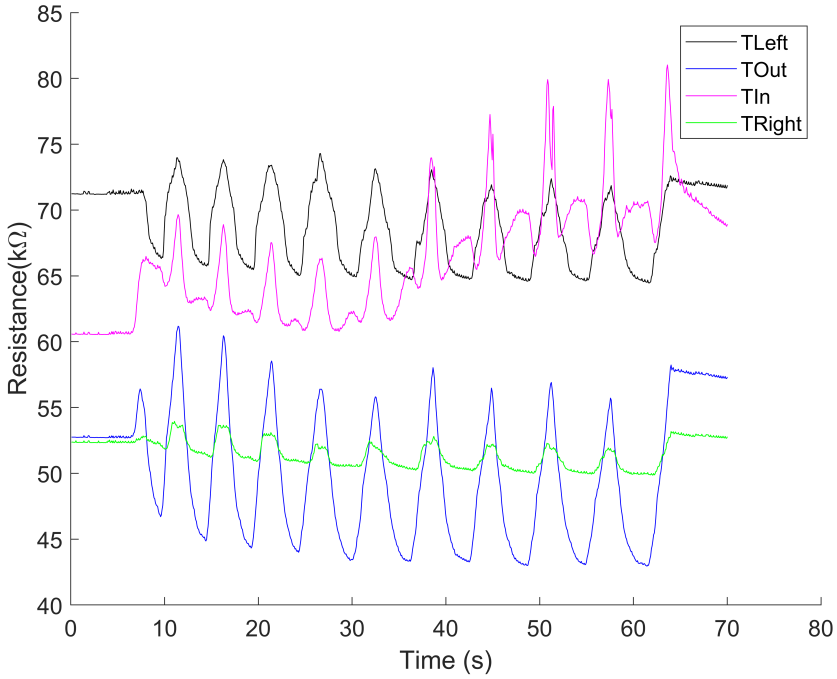

Figure 42 Resistance plot for the top outward repeated bend

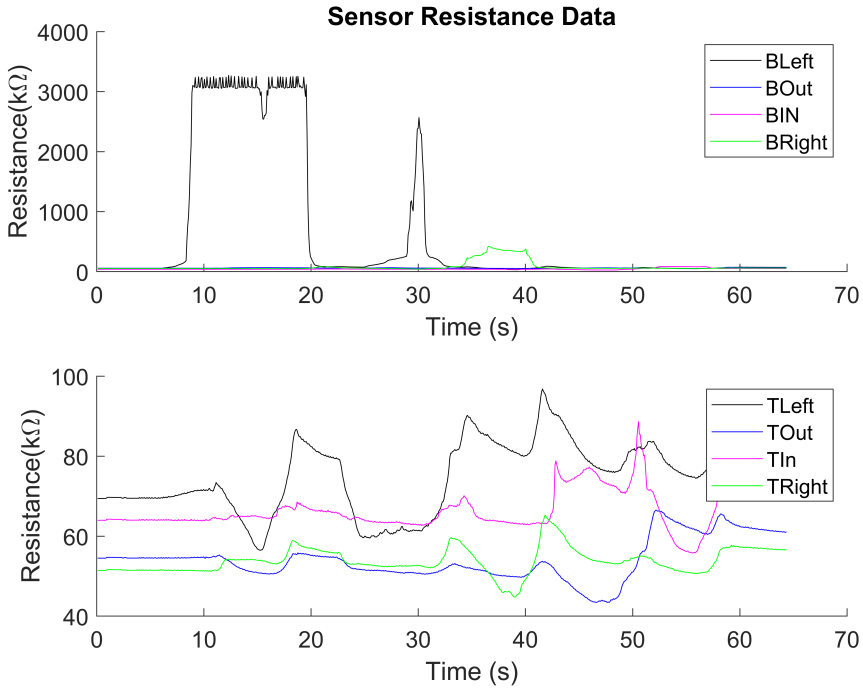

Figure 43 Resistance plot for the full joystick S-shape experiment

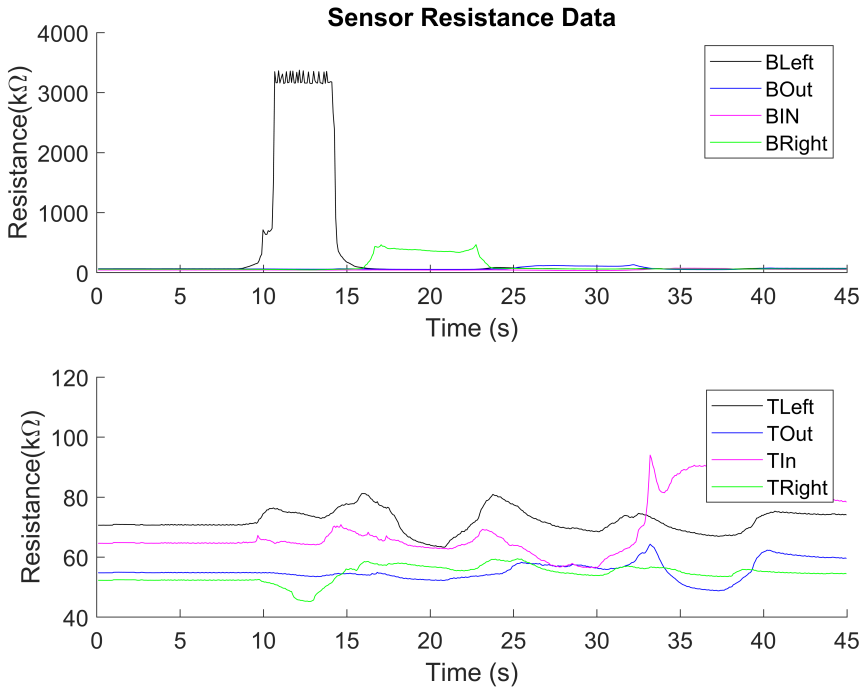

Figure 44 Resistance plot for the full joystick C-shape experiment

C Used software

During the preparation of this work the author used Copilot (Microsoft, USA) (based on ChatGPT 4.0) for the following purposes: software (MATLAB, Solidworks, Arduino IDE) troubleshooting, use as a general search engine, LateX code writing. After using this tool/service, the author(s) reviewed and edited the content as needed and take(s) full responsibility for the content of the work.

Other software that was used includes:

- SolidWorks: modelling the joystick and its components.
- MatLab: writing G-code for the CTPUC printing, interfacing with the Arduino to read the sensor data
- Arduino IDE: writing code to the Arduino to allow reading of sensors.